eSTAR: A Letter of Intent

The STAR Collaboration

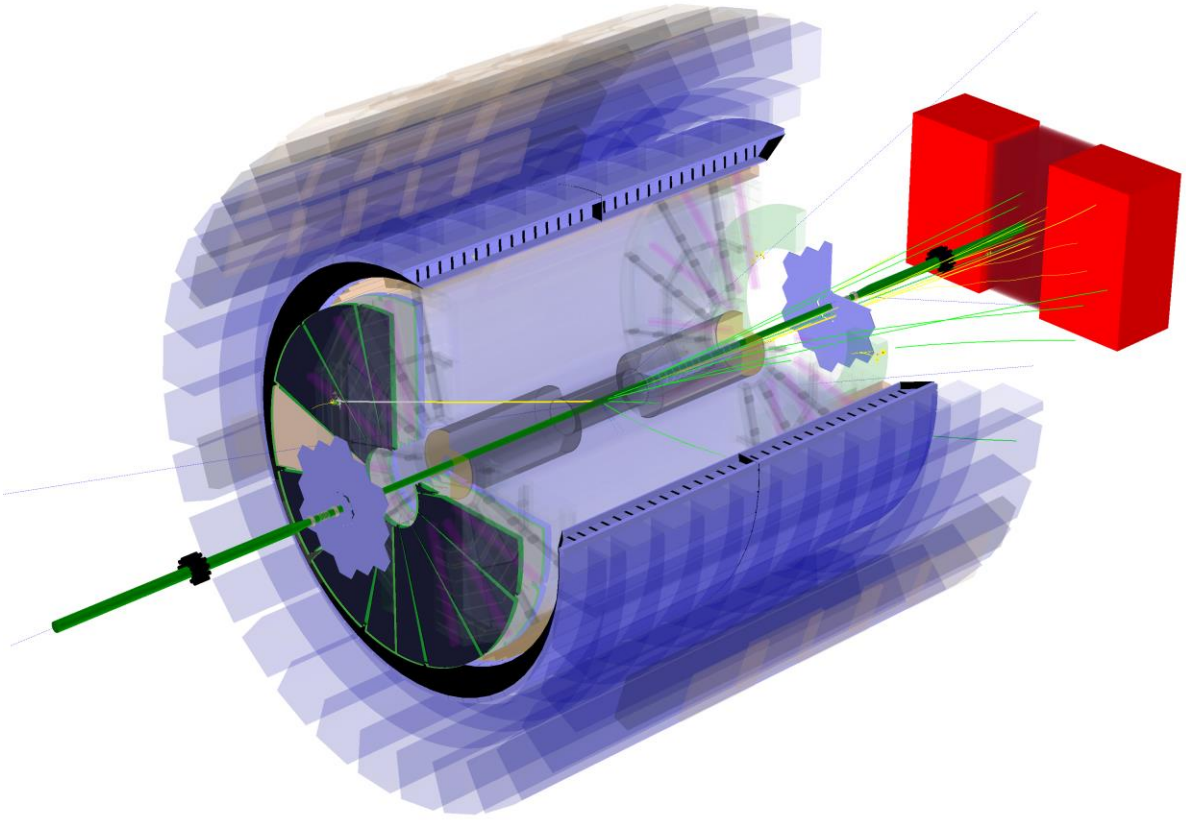

September 2013

This page is intentionally left blank.

Executive Summary

In this Letter of Intent, the STAR collaboration proposes a path to evolve STAR into a major experiment, referred to as eSTAR, at a possible future Electron-Ion Collider (EIC) at Brookhaven National Laboratory, eRHIC. A core component of this plan is a suite of optimized detector upgrades to maintain and extend the existing low-mass mid-central rapidity tracking and particle-identification capabilities towards forward rapidity to enable the precision deep-inelastic-scattering measurements that form the experimental foundation of the EIC science program. This Letter of Intent is submitted in response to a May 2013 charge by BNL Associate Laboratory Director Berndt Mueller, which is reproduced in the Appendix to this Letter.

We demonstrate through simulations that eSTAR will deliver on a broad range of key measurements:

- inclusive structure functions in (polarized) electron-nucleon and electron nucleus scattering,
- semi-inclusive observables that have one or more identified particles in the current fragmentation region and dihadron correlations in the low-x regime,
- exclusive observables in deeply-virtual Compton scattering and in vector meson production processes, including diffractive processes.

These measurements have been identified as flagship science cases in the recent EIC community white-paper for the eRHIC facility specifications envisioned in the charge for this LOI. These specifications include collisions of a polarized electron beam of up to 10 GeV energy with the existing ion and polarized proton beams in the RHIC Blue ring at respective instantaneous luminosities of 6×10^{32} cm^{-2} s^{-1} and $1\text{x}10^{33}$ cm^{-2} s^{-1} and readiness for physics in the mid-2020s.

The baseline eSTAR plan has three essential upgrade projects for the scientific program, consisting of endcap Time-of-Flight walls located between the TPC and the magnet pole-tips on the East and West sides of the interaction region (ETOF and WTOF, covering the regions $1 < |\eta| < 2$ in pseudo-rapidity), a GEM-based Transition Radiation Detector (GTRD) between the TPC and ETOF in the forward electron direction, covering $-2 < \eta < -1$, and a Crystal ElectroMagnetic Calorimeter with preshower (CEMC, covering $-4 < \eta < -2$). Furthermore, eSTAR will rely on a replacement upgrade of the Inner Sectors of the existing Time-Projection-Chamber prior to a completion of the RHIC Beam-Energy Scan program with $A + A$ collisions and on a subsequent upgrade in the form of a new Forward Calorimeter System (FCS) with associated Forward Tracking System (FTS) on the West side of STAR. The upgrade sequence will enable STAR to complete the high-priority experimental programs with $A + A$, polarized $p + p$, and $p + A$ collisions outlined in its decadal plan, and provide a natural transition to eRHIC as well as essential detector components for eSTAR. The total project cost for these upgrades is anticipated to be $42 M. The interaction-region design is anticipated to be conceptually similar to the crab-crossing design in the EIC white-paper, with suitable optimization for, and integration with, a finalized eSTAR design. This holds also for the methods and instrumentation to measure luminosity and polarization.

The STAR collaboration presently consists of more than 500 scientists from 53 institutions of which 23 are institutions in the United States. The majority of the collaboration is strongly supportive of the eSTAR effort and multiple institutions are already actively engaged in simulations and R&D for each of the envisioned upgrade projects. The detector configuration presented in this Letter of Intent represents the baseline instrument. New collaborators from the broader community are vitally important. Science-driven proposals, for instance, in the areas of displaced vertex detection and forward particle-identification, to further strengthen the baseline eSTAR scientific capabilities and program, are particularly welcome.

Contents

1 Introduction

STAR, as the one large acceptance detector at RHIC, has the advantage of full azimuthal angle coverage, TPC tracking within $|\eta|<1.0$ and particle identification through Time-of-Flight. The central Barrel and End-cap Electro Magnetic Calorimeters (BEMC and EEMC), when combined with charged particle tracking from the TPC, provide coverage for measurements of electrons, photons, neutral pions, and jets. Based on these unique capabilities, STAR has developed a $p + p$, $d(p) + A$ and $A + A$ program[1] that drives the RHIC science program during the current decade and addresses the overarching questions defined for the subfield of Quantum Chromodynamics (QCD) in the 2007 Nuclear Physics Long Range Plan[2].

The STAR experiment has already addressed many of these questions over the last years with measurements in $A + A$, $d + A$ and (un)-polarized $p + p$ collisions. Some of the latest, most striking results, closely related to the core physics program of a future electron-ion-collider (EIC)[3], are listed here. Polarized $p + p$ collisions have set the most precise constraints to date on the polarization of the gluons in the proton. New global analyses, which include results both from PHENIX (π^0 A_{LL}) and STAR (jet A_{LL}) indicate that the integrated contribution to the proton spin from gluons in the momentum range $0.05 < x < 0.2$ is 20%. This should be compared to the 30% quark contribution in the quark momentum range $0.001 < x < 1.0$. The STAR preliminary results on A_L^{W+} taken during 2012 have been included in a pQCD-fit and show clear improvement on the determination of the polarization of the light sea quarks and their integral for $\Delta\bar{u}$ and $\Delta\bar{d}$ in the range $0.05 < x < 1$ at Q^2=10 GeV^2. For $\Delta\bar{u}$, a shift away from the current best mean value is observed, reflecting that the new STAR A_L^{W-} data lie above the central value based on a fit to the world data. Already, with only the preliminary 2012 STAR data, the new global analysis shows a preference for $\Delta\bar{u} > \Delta\bar{d}$ in the range $x > 0.05$. The observation of a dramatic broadening of forward π^0-π^0 correlations in d + Au collisions provides the clearest indication to date that the onset of gluon saturation is accessible at RHIC. Related theoretical developments point to a potential connection between gluon saturation and a longitudinally extended correlation called "the ridge", which was first observed by STAR in Au+Au collisions.

Significant advances have been made in quantifying the properties of the Quark Gluon Plasma. The measurement of the viscosity to entropy ratio very close to the quantum limit of $1/4\pi$ has had a major impact beyond the nuclear physics community. Measurements of the non-photonic electron R_{AA} indicate that even hadrons containing heavy quarks are suppressed in central Au + Au collisions, thus motivating further understanding of the partonic energy loss mechanism(s) in nuclear matter. The higher harmonic decomposition of particle azimuthal momentum distributions have identified novel characteristics in heavy-ion collisions relative to $p + p$, including the near-side “ridge” related to quantum fluctuations in the early state that are propagated through a low viscosity plasma phase, into the final state. Ultra-peripheral heavy-ion collisions utilize the high-flux of high-

energy Weizsäcker-Williams photons to mimic electron-ion collisions and provide a first-glimpse and proof of principle of exclusive diffractive vector meson production. RHIC has completed an initial beam energy scan program with center-of-mass beam energies down to 7.7 GeV. Many results are still forthcoming, but completed measurements already point towards the increasing dominance of hadronic interactions at the lower center-of-mass energies consistent with the long sought after direct evidence for a change in the degrees of freedom.

In the coming years, the STAR detector system will continue to evolve through several upgrades towards superior detection capabilities and/or broader kinematic coverage that will position STAR well for the $p + p$, $p + A$ and $A + A$ measurements and at the initial phase of an EIC. These upgrades are described in short in the following and in more detail in Section 3.

The Heavy Flavor Tracker (HFT) and Muon Telescope Detector (MTD) will be essential to quantify the properties of the strongly-coupled Quark-Gluon Plasma created in high energy heavy ion collisions through heavy quarks, which represent excellent controllable probes for these investigations. Upgrades to both the trigger and the data acquisition system will also be required[1]. To enhance the STAR capabilities for the Phase-II RHIC beam energy scan, an upgrade of the inner sectors of the STAR TPC (iTPC) is proposed. Increasing the segmentation on the inner pad plane will provide better momentum resolution, better dE/dx resolution, and most importantly will extend the acceptance up to rapidity $|\eta| < \sim 1.7$ compared to the current TPC configuration of $|\eta| < \sim 1.0$. This increase in acceptance will enable STAR to better measure the longitudinal extent of the ridge which provides the best means to disentangle contributions to the correlations from various stages of the collisions such as the initial state, the plasma phase and freeze-out. This separation of contributions is essential for a completely accurate determination of the plasma viscosity in $A + A$ collisions and provides a means to measure the de-coherence of flux-tube like structures with increasing rapidity in $p + A$ and $A + A$ collisions. Uncertainties in the initial incoming parton flux and the details of the geometrical fluctuations remain, which constitute a major scientific goal for our future pA and AA physics program. Upgrades will also be necessary to take advantage of the opportunities presented by $p + p$ and $p + A$ collisions at RHIC. Upgrades to the current forward ($3<\eta<4$) electromagnetic calorimeter are needed to provide e/h and γ/π^0 discrimination. This will allow first studies to unravel the origin of the large transverse spin asymmetries and the partonic structure of heavy nuclei. A further upgrade of the STAR forward detection system will combine a high-resolution tungsten-powder electromagnetic calorimeter with a high resolution hadronic calorimeter (in the following abbreviated FCS) and forward tracking system (abbreviated as FTS), which are needed to give definite answers on the origin of the large transverse spin asymmetries at high x_F, as well as the question whether heavy nuclei have saturated gluon distribution in the initial state. The upgrades will, through double spin asymmetries in forward di-jet production, constrain the shape and the magnitude of the gluon helicity distribution at low parton momentum x. An upgrade to the current Roman pot system will permit a high-sensitivity search for glueballs, the study of exclusive and diffractive reactions in $p + p$, and (un)-polarized $p + A$ collisions, which will allow one to study generalized parton distributions through exclusive J/Ψ -production.

The above described current and future STAR physics program and detector capabilities are well aligned with the science goals of the EIC as described in the recent EIC white paper[3]. An Electron Ion Collider is being considered as the next generation national QCD facility in nuclear physics. The most intellectually pressing questions that an EIC will address that relate to our detailed and fundamental understanding of QCD in this frontier environment are:

1. How are the sea quarks and gluons, and their spins, distributed in space and momentum inside the nucleon? How are these quark and gluon distributions correlated with overall nucleon properties, such as spin direction? What is the role of the orbital motion of sea quarks and gluons in building the nucleon spin?
2. Where does the saturation of gluon densities set in? Is there a simple boundary that separates this region from that of more dilute quark-gluon matter? If so, how do the distributions of quarks and gluons change as one crosses the boundary? Does this saturation produce matter of universal properties in the nucleon and all nuclei viewed at nearly the speed of light?
3. How does the nuclear environment affect the distribution of quarks and gluons and their interactions in nuclei? How does the transverse spatial distribution of gluons compare to that in the nucleon? How does nuclear matter respond to a fast moving color charge passing through it? Is this response different for light and heavy quarks?

Answers to these questions are essential for understanding the nature of visible matter.

An EIC is the ultimate machine to provide answers to these questions for the following reasons:

1. A collider is needed to provide kinematic reach well into the gluon-dominated regime;
2. Electron beams are needed to bring to bear the unmatched precision of the electromagnetic interaction as a probe;
3. Polarized nucleon beams are needed to determine the correlations of sea quark and gluon distributions with the nucleon spin;
4. Heavy ion beams are needed to provide precocious access to the regime of saturated gluon densities and offer a precise dial in the study of propagation-length for color charges in nuclear matter.

The addition of the envisioned electron beam to the RHIC hadron facility (eRHIC) will accomplish the machine requirements for an EIC as listed above.

2 eSTAR Capabilities to Explore the EIC Scientific Highlights

The science case for a high-energy polarized Electron-Ion Collider (EIC) in the U.S. has been developed and is described in a recent community white paper[3]. One of the possible paths to realize an EIC envisions an energy-staged electron beam upgrade to the RHIC facility, eRHIC. In the following, we give our initial assessment of the main measurement capabilities afforded by a suitably evolved STAR experiment, eSTAR, at an initial stage (phase-I) of eRHIC.

The core of the STAR[4] experiment, consisting of the Time Projection Chamber (TPC) and surrounding detector subsystems inside a 0.5T solenoidal field, is maintained in the eSTAR detector. It is complemented with upgrades along the electron-beam direction in the form of a compact transition-radiation detector (TRD) and Endcap time-of-flight system (E/WTOF), which serve primarily to enhance the detection capabilities for the electrons scattered at rapidities between -1 and -2, and a high-resolution crystal calorimeter (CEMC) with a pre-shower detector to detect and measure with precision the scattered electrons at more forward rapidities. These upgrades, and upgrades prior to the eRHIC era, in particular the upgrade of the TPC inner sectors and a forward calorimeter system (FCS, consisting of EMCAL and HCAL) with an associated tracker (FTS), are described in more detail in Section 3. The FCS and FTS will enable the reconstruction of photons, neutral pions, and charge-identified hadrons in semi-inclusive observables in a kinematic regime that connects the current measurements in fixed target kinematics with the collider kinematics of eRHIC. Furthermore, it will aid the identification of diffractive events, and has considerable acceptance for hadrons produced in scattering events where the electron cannot be measured with precision and the event kinematics must be reconstructed from the hadronic final state.

The EIC scientific program[3] is made possible by accelerator machine performance, and experimental measurement capability for inclusive, semi-inclusive, and exclusive deep-inelastic scattering events, as well as for diffractive events. The remainder of this section is organized accordingly.

2.1 Machine Performance

In accordance with the charge from the Brookhaven National Laboratory Associated Laboratory Director (Appendix), eRHIC (phase-I) is assumed to deliver:

- electron beams with energies of up to 10 GeV and 70% polarization,
- hadron beams as currently available at RHIC, thus including in particular:
    - polarized proton beams with energies of up to ~250 GeV,
    - heavy-ion beams from deuteron to gold with energies of up to 100 GeV/nucleon,
- instantaneous luminosities of $1\text{x}10^{33}$ $\text{cm}^{-2}\text{s}^{-1}$ for $e+p$ and $6\text{x}10^{32}$ $\text{cm}^{-2}\text{s}^{-1}$ for $e+Au$ collisions at the respective top energies.

The above luminosities are assumed to scale inversely proportional to the hadron beam energy and to be constant with electron beam energy for the range of nuclei and energies under consideration. The interaction region (IR) design for eSTAR is anticipated to be similar in layout to that shown in Figure 5.4 of the EIC white paper. However, due to the length of the envisioned eSTAR detector, the beam elements closest to the IR will have to be placed at 8m from the nominal interaction point instead of the 4.5m described in the EIC white paper. This is expected to degrade the luminosities available to eSTAR by a factor of about two. The sharing of beam with one other eRHIC IR is anticipated to result in a reduction of the luminosity available to eSTAR by an additional factor of two compared to the values stated above.

Delivered integrated luminosities of 1 fb^{-1} for any of the beam energies and species at both IRs are thus well within the range of the initial eRHIC beam-operation periods and we have, unless stated otherwise, taken this value as a basis for our assessment of the eSTAR physics performance below.

The accelerator and IR designs are integral aspects to the eSTAR performance. The eSTAR IR design is assumed to follow the crab-crossing design described in the EIC white paper. We envision an active optimization for achieving maximum eSTAR performance in the future, possibly involving modest reconfiguration of some of the eSTAR forward detector subsystems. The techniques to determine luminosity and polarization are, likewise, assumed to closely follow those described in the EIC white paper and to result in adequate accuracy.

2.2 Physics Performance

In deep-inelastic scattering events, a virtual photon, W, or Z boson is exchanged in the scattering of a beam lepton (electrons in the case of eRHIC) and a target proton or nucleus. The simulations in this section focus on reactions in which a virtual photon is exchanged. The event kinematics, in terms of the invariants Bjorken-x, the photon virtuality Q^2, and the inelasticity $y=Q^2/(x\,s)$ where $\sqrt{s}$ is the center-of-mass energy, can be fully reconstructed from the known beam energies and measurement of the scattered electron. Alternatively, the event kinematics can be reconstructed from measurements of the hadronic final state produced in the scattering, or from a combination of scattered lepton and hadronic observables.

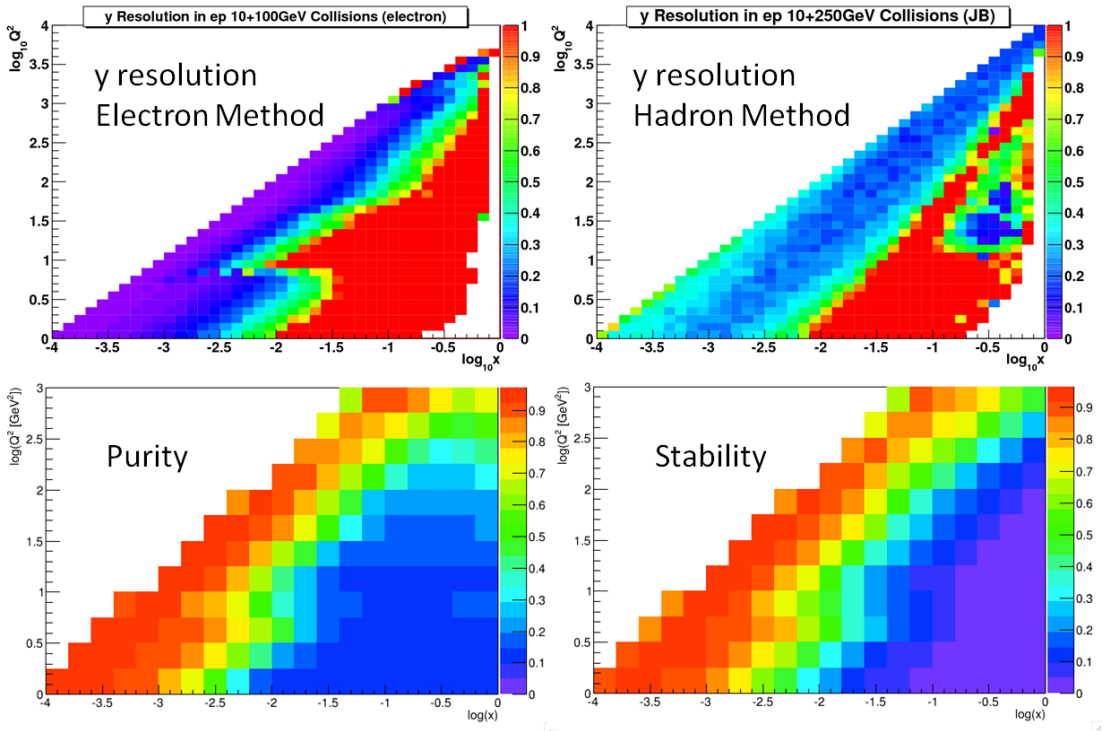

Figure 2.1: (Top) The simulated resolution in y for different values of x and Q^2 in the eSTAR acceptance for the deep-inelastic scattering of 10 GeV *electron beams off 250* GeV *proton beams when y is reconstructed from measurements of (left) the scattered electron and (right) the hadronic final state. (Bottom) The corresponding purity (left) and simulated bin-survival-probability (right) for different values of x and Q^2 in the eSTAR acceptance when the event kinematics are reconstructed from the scattered electron.*

Figure 2.1 illustrates the eSTAR acceptance in x and Q^2 and the effects of finite measurement resolutions for the case of an electron beam energy of 10 GeV and a proton beam energy of 250 GeV. The overall characteristics for other combinations of beam energies are similar. We focus here mostly on measurements in which x, Q^2, and y are reconstructed through the measurement of the scattered electron. The resolutions in x and y inevitably worsen with decreasing y. These characteristics and the corresponding effects on purity (defined as the ratio of the number of events reconstructed in a given bin to the number of events generated in the same bin) and stability (defined by the fraction of generated events that is reconstructed in the same bin) or bin-survival probability are clearly seen in Figure 2.1. They are common to all deep-inelastic scattering measurements discussed in this section.

2.2.1 Inclusive Measurements

Unpolarized measurements

A key goal of the EIC is the precise determination of the inclusive structure functions F_2 and F_L over a wide and resolved kinematic range in x and Q^2 and for various nuclei to study nuclear parton

distributions and their expected saturation for low values of x. The inclusive structure functions F_2 and F_L are related to the (reduced) one-photon-exchange cross-section:

$$\sigma_r = \frac{d^2\sigma}{dxdQ^2}\frac{x\,Q^4}{2\pi\alpha^2[1+(1-y)^2]} = F_2(x,Q^2) - \frac{y}{1+(1-y)^2}F_L(x,Q^2)$$

and can be resolved from measurements at equal x and Q^2 for different y in a so-called Rosenbluth separation analysis. This entails measurements at different beam energies.

To assess the eSTAR capabilities in measuring $F_2(x,Q^2)$, a Rosenbluth separation analysis was performed on simulated data to extract F_2 and F_L. Pseudo-data were generated for different incident electron beam energies of 5 and 10 GeV and Au beam energies of 50, 75 and 100 GeV per nucleon using PYTHIA with the EPS09 LO PDFs for Au. The eSTAR fast detector response, discussed in detail in Section 4, was applied to the scattered electron. The reduced cross-section as seen in the eSTAR acceptance was extracted for different values of x and Q^2 from the simulated data for 50, 75, and 100 GeV/nucleon *Au* beams and 5 and 10 GeV incident electron beams. The pseudo-data correspond to an integrated luminosity of 1fb^{-1} for each of the combinations of beam energies. The actual measurements will be dominated by systematic uncertainties.

The values extracted for $F_2(x,Q^2)$ are shown for both electron beam energies in Figure 2.2. Point-to-point systematic uncertainties of 3%, consistent with the values achieved at the HERA experiments, were included in the pseudo-data and a minimum lever arm in $y/[1+(1-y)^2]$ of 0.1 was imposed in the extraction of $F_2(x,Q^2)$.

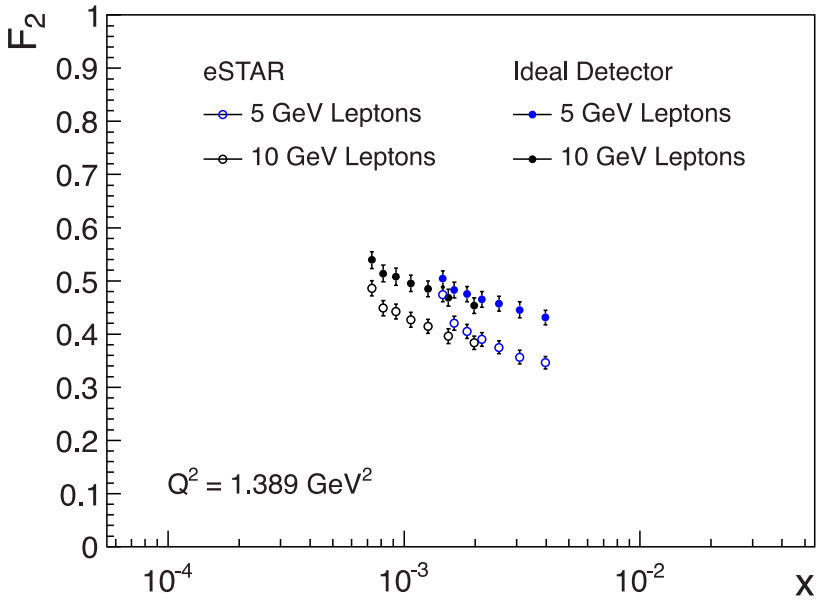

Figure 2.2: Projected measurements of the unpolarized inclusive structure function $F_2(x,Q^2)$ in deep-inelastic scattering of electrons of the indicated energies with Au nuclei of 50-100 GeV/*nucleon energies to study nuclear parton distributions and their saturation at low values of Bjorken-x. The eSTAR projections before acceptance and efficiency correction are shown in comparison with those for an ideal projection.*

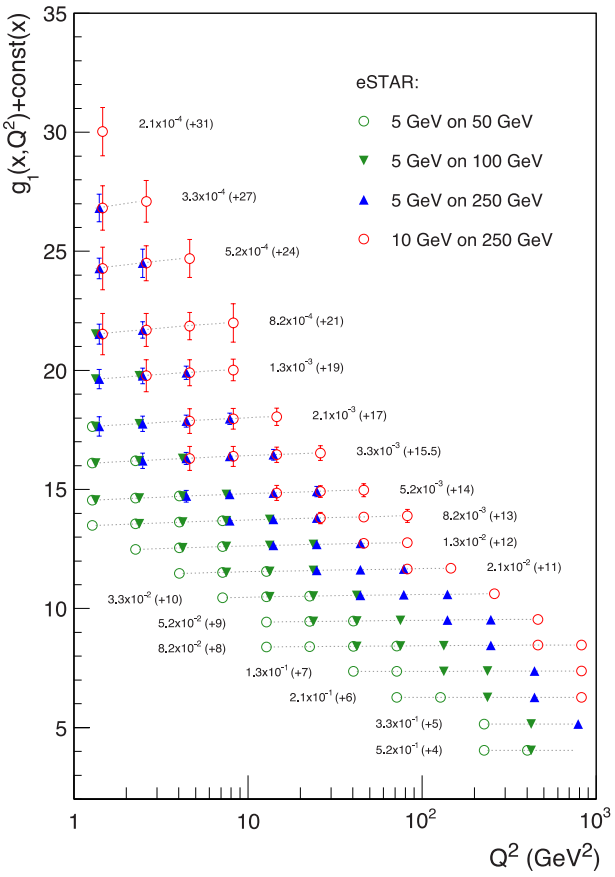

Figure 2.3: eSTAR pseudo-data on the inclusive spin structure function $g_1(x,Q^2)$ versus Q^2 at constant x for 5 and 10 GeV *longitudinally polarized electron beams colliding with 50, 100, and 250* GeV *longitudinally polarized proton beams at eRHIC, as indicated. The projected uncertainties are statistical only. The data for each of the indicated x values is offset by the constant in brackets for clarity. The dotted line indicates the central value of the DSSV expectation.*

The comparison of the values extracted for $F_2(x,Q^2)$ with eSTAR and with an ideal detector in Figure 2.2 shows large and similar acceptance in Bjorken-*x*. The vertical offset between the sets of data results from differences in acceptance and resolution. These effects can and would be corrected in actual measurements using full detector acceptance and response simulations.

A key goal of the EIC for polarized deep-inelastic scattering is the precise determination of the inclusive spin structure function g_1 of the nucleon over a wide and resolved kinematic range in x and Q^2. A perturbative QCD analysis of $g_1(x,Q^2)$ at an EIC is anticipated to give definitive insight into the size and distribution of the quark and gluon spin contributions to the nucleon spin.

The projected eSTAR measurement capabilities for $g_1(x,Q^2)$ are shown in Figure 2.3 for integrated luminosities of 1 fb^{-1} at each of the energies and 70% beam polarizations. The analysis methods are

different from the analysis of the spin-independent structure functions F_2 and F_L in that they do not necessitate a Rosenbluth separation analysis. Spin-dependent analyses, however, do impose stringent demands on purity and stability. The results shown in Figure 2.3 impose a minimum purity of 80%, an upper value on y of 0.9 to reduce sensitivity to radiative backgrounds in the measurement, and a limit of 0.1 on the depolarization of the exchanged photon. The latter is positively correlated with y and in effect imposes an approximate threshold of $y > \sim 0.1$.
The eSTAR capabilities for measurements of $g_1(x,Q^2)$ will thus cover a wide region in x and Q^2, well beyond that achieved by existing fixed-target measurements. For $0.001 < x < 0.2$, the eSTAR data offer a lever arm of one decade or more in Q^2 and will enable precision QCD analysis to determine the quark and gluon spin distributions in the polarized nucleon.

2.2.2 Semi-Inclusive Measurements

In semi-inclusive deep-inelastic scattering measurements, one or more of the final-state particles produced in the collision are detected and measured in addition to the scattered lepton. The primary goals of 1-particle semi-inclusive deep-inelastic scattering measurements at an EIC include a full flavor separation of the polarized quark and anti-quark distributions in the polarized nucleon, the study of polarized and unpolarized transverse-momentum-dependent (anti-)quark and gluon distributions and their scale dependences, and the precision study of hadronization and energy loss in cold nuclear matter. Two-particle correlation measurements have traditionally been used to probe gluon distributions by means of their significant scattering contributions from photon-gluon fusion processes and have been proposed as a robust probe of gluon saturation in nuclei at an EIC.

The requirements to identify and measure the scattered lepton in semi-inclusive deep-inelastic scattering measurements are essentially the same as those for inclusive measurements. However, additional acceptance requirements are imposed by the need to measure and identify the final-state hadrons. The final-state hadrons in 1-particle semi-inclusive deep-inelastic scattering measurements are typically characterized by their transverse momenta, p_T, with respect to the virtual photon that is exchanged in the interaction, by their energy fractions, z, and by their angles with respect to the reaction plane as well as the hadron spin direction in the case of polarized measurements.

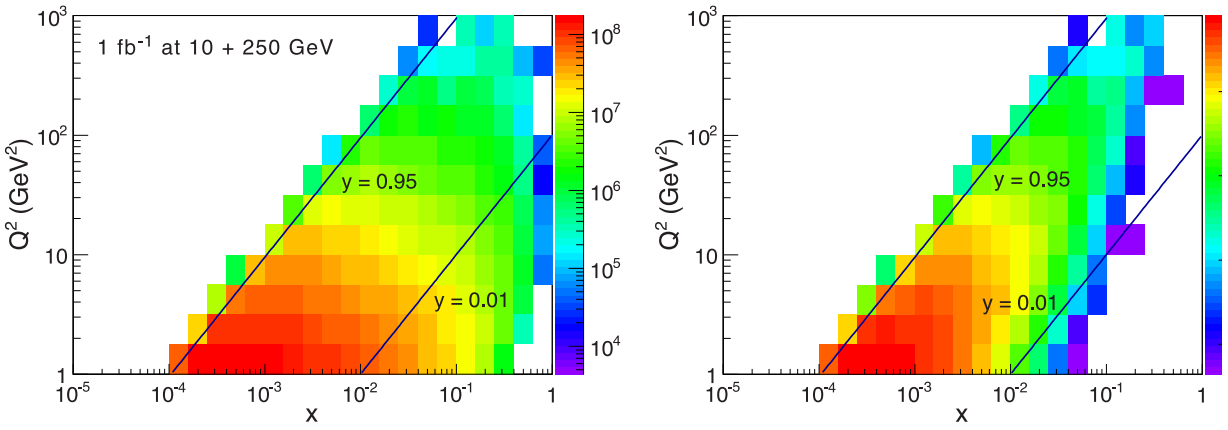

Figure 2.4: (x, Q^2) distributions from generator (left) and after eSTAR charged pion PID acceptance (right).

Figure 6.2 in the EIC white paper[3] shows the combined momentum and rapidity distributions in the laboratory frame for pion production in non-exclusive reactions. The range of existing STAR capabilities listed in Table 3.1 and Table 3.2 covers $|\eta| <$ ~1.7 over the entire momentum range for pions. The capabilities for identified kaons span a smaller range in p of up to about 4 GeV. The existing STAR TPC and TOF will be maintained in eSTAR and will be complemented with forward time-of-flight coverage to provide adequate start-time resolution. eSTAR is thus projected to have significant 1-particle semi-inclusive deep-inelastic scattering measurement capabilities to delineate the spin-flavor structure of the nucleon. Figure 2.4 shows the SIDIS process in (x, Q^2) phase space with generator output (left panel) and the distribution after eSTAR PID acceptance requirement for charged pions (right panel). The resolutions in transverse-momentum-dependent measurements remain to be quantified explicitly through simulations.

Parton Energy Loss in the Nuclear Medium

Collisions of electron beams with ion beams of various species at an EIC make it possible to study with the precisely resolved kinematics of 1-particle semi-inclusive deep-inelastic scattering processes the mechanisms by which quarks and gluons lose energy and hadronize in cold nuclear matter. This is complementary to the studies of jet quenching in heavy-ion collisions, whereby a fast moving color charged parton loses energy in a hot and dense quark-gluon plasma, which is among the major discoveries of the RHIC physics program.

We have carried out Pythia-based fast simulations of the eSTAR response for 5 GeV and 10 GeV electron beams with 50 and 100 GeV/nucleon hadron beams, following closely the presentation of

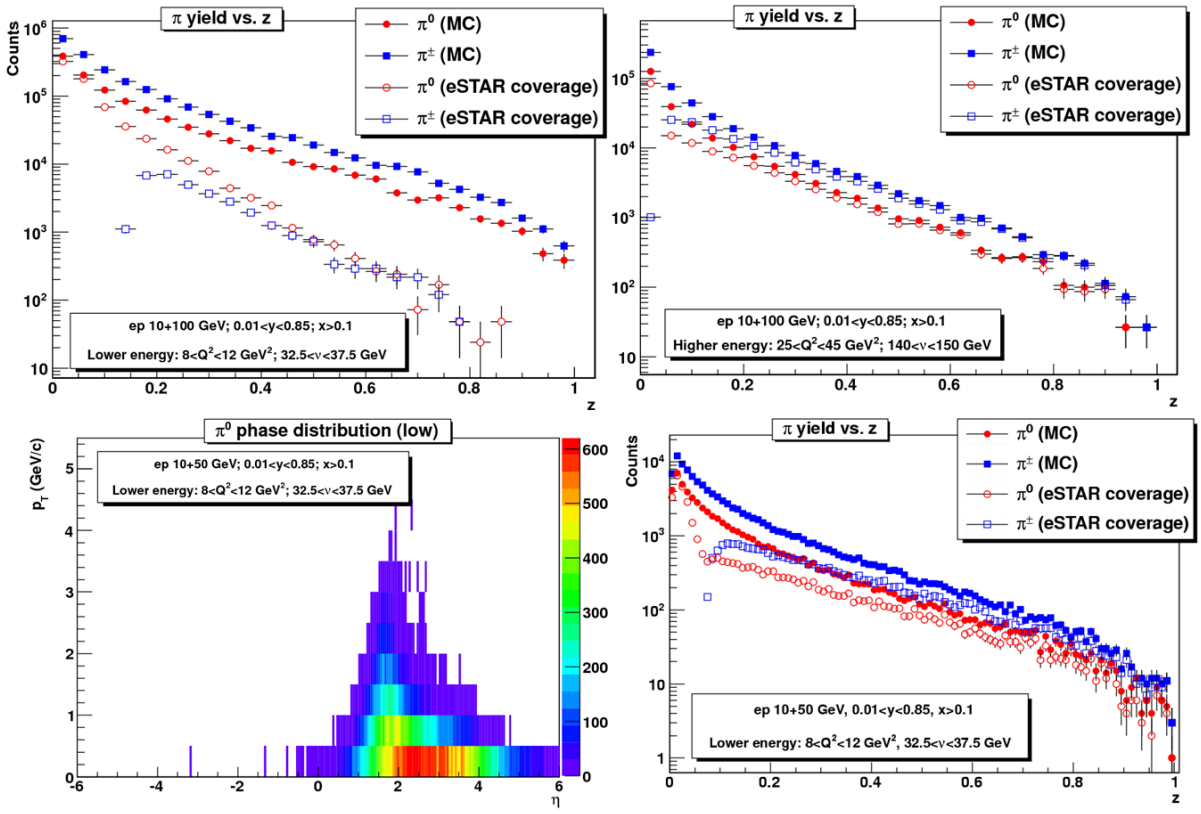

Figure 2.5: The eSTAR acceptance for charged and neutral pion production versus the fragmentation momentum fraction z for partons with high (top left) and low (top right) energies in deep-inelastic scattering collisions of a 10 GeV *electron beam with a 100* GeV *hadron beam. The lower panels show (left) the combined rapidity versus transverse momentum distribution and (right) the corresponding z-spectrum in 10* GeV *on 50* GeV *collisions. The samples presented here correspond to1* fb^{-1} *integrated luminosity that serves as a baseline in our other simulations.*

energy-loss studies in cold nuclear matter in the EIC white paper. Figure 2.5 shows the resulting acceptance for high and low values of the photon virtuality Q^2 and energy ν. These regions are thought to probe hadronization of the parton outside and inside the nuclear medium. The difference between the generator level and eSTAR observed distributions are caused primarily by the

acceptance gap for π^0 rapidities between 2.0 and 2.5 and the lack of π^{+-} identification in the forward hadron region. Significant capability is seen to exist despite these limitations.

Dihadron correlations

Dihadron correlation measurements, that is, measurements of the two-particle semi-inclusive deep-inelastic scattering process $e + A \rightarrow e' + h_1 + h_2 + X$, offer access to gluon distributions via scattering contributions from photon-gluon-fusion processes. The nonlinear QCD evolution of multi-gluon distributions is expected to be different from that of the single-gluon distribution and can be measured through modification of the di-hadron correlation distributions[5]. Saturation models predict the functional form of the multi-gluon distribution as functions of the gluon transverse momentum, k_T, and the saturation momentum, $Q^2_s(x)$[6,7].

The left panel of Figure 2.6 shows the spectrum of the difference $\Delta\phi$ in azimuthal angle between a trigger-hadron with momentum $p_T^{trig} > 2$ GeV and an associate-hadron with momentum $p_T^{trig} > p_T^{assoc} > 1$ GeV. The projected eSTAR precision is shown together with theoretical expectations.

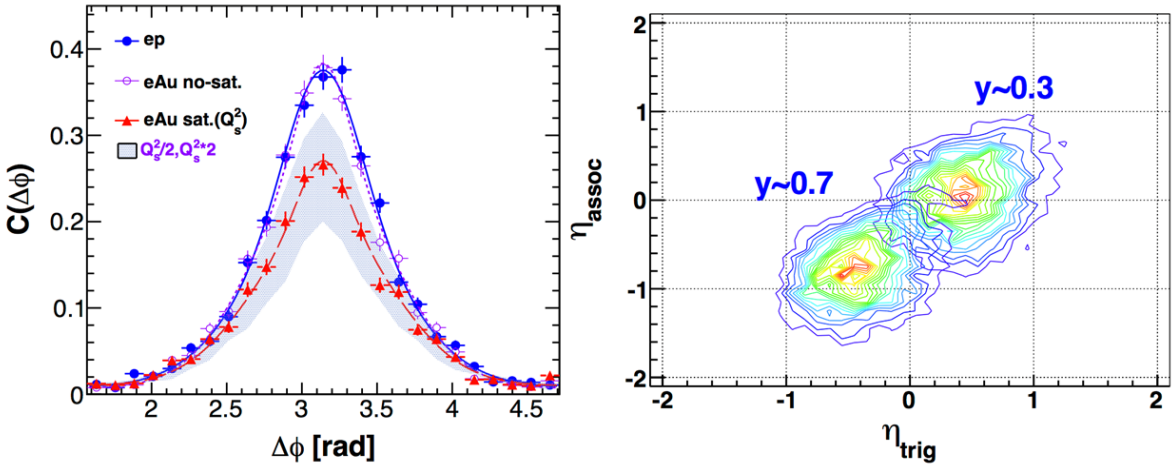

Figure 2.6: Left panel: Azimuthal angle differences $\Delta\phi$ of two hadrons at Q^2 =1 GeV^2 an integrated luminosity of 1 fb^{-1} in e+p (solid circles) and e+Au (open circles) scattering of a 10 GeV electron beam off a 100 GeV/nucleon hadron beam for saturated and conventional non-saturated models. Right Panel: Pseudorapidity (η) distributions of two hadrons at Q^2 = 1 GeV^2 and y~0.3, 0.7.

The eSTAR projected precision was evaluated for an integrated luminosity of 1 fb^{-1} in $e + p$ and in e + Au collisions with 10 GeV electron beams and 100 GeV/nucleon hadron beams. The expectations are saturation model predictions and conventional non-saturated correlation functions. The prediction of the difference can be clearly differentiated in eSTAR measurements, considering even the uncertainties in the expectation caused by uncertainty in the saturation scale as shown by the band. The final-state hadron pairs are produced near mid-rapidity as shown in the right panel of Figure 2.6. The eSTAR mid-rapidity capabilities are thus well suited for this measurement at eRHIC (phase-I) energies.

2.2.3 Exclusive and Diffractive Measurements

The study of exclusive inelastic and exclusive diffractive processes requires reconstruction of the scattered electron, the scattered beam hadron (either intact or dissociated), and the final-state particle(s) produced in the interaction. In the region of low-x, the beam proton, if it remains intact, scatters at such a small angle that its measurement requires forward detectors installed in Roman Pots along the beam pipe. In diffractive $e + A$ collisions, the scattered ion is closer to the beam and typically cannot be measured. The reconstruction of the final-state particle(s), typically a photon or a vector meson decaying into leptons or low-momentum hadrons, imposes additional detector requirements on tracking, particle identification and calorimetry. While these are key measurements in $e + p$ and $e + A$ collisions, there are significant challenges an EIC detector needs to overcome.

The objective of these measurements with an EIC is to provide spatial imaging of quarks and gluons in the (polarized) nucleon and in nuclei. The reaction channels of main EIC interest are deeply-virtual Compton scattering (DVCS), $e + p \rightarrow e' + p' + \gamma$ and the exclusive production of a J/ψ, φ, or ρ vector meson, $e + p \rightarrow e' + p'$ + vector meson. These reactions are described in terms of Generalized Parton Distributions (GPDs), which in turn describe the 1+2D distribution of longitudinal momentum and transverse spatial distribution of the target nucleon/nucleus.

Coherent diffractive events, $e + h \rightarrow e' + h' + X$, in $e + p$ and $e + A$ scattering are closely related. This holds also for incoherent diffractive processes, in which the hadron breaks up. In both cases, the events feature a characteristic rapidity gap that is free of particles. These events are indicative of a color-neutral t-channel exchange between the virtual photon and the hadron over several units in rapidity. These measurements at an EIC will be used to probe gluon saturation in a new regime of QCD. A day-one measurement of inclusive diffractive cross-section to total cross-section as shown in Fig.1.6 in the EIC white paper[3] is anticipated to be feasible also with eSTAR. In the later part of this section, we perform an evaluation of a more exclusive measurement of coherent diffractive vector meson production.

Deeply Virtual Compton Scattering

The MILOU generator[8], combined with the eSTAR response parametrizations, has been used to assess the eSTAR capabilities for DVCS measurements. The electrons are detected with tracking detectors or calorimeters, which serve also for the detection of photons. Instrumented Roman Pot stations are used to detect the scattered proton over an assumed range of $0.03 < |t| < 2$ GeV^2 and the exclusivity of the event will be ensured by full azimuthal coverage in $-4 < \eta < 5.2$. eSTAR offers good acceptance in (x, Q^2), which is essential in the study of evolution effects predicted by perturbative QCD theory and to extract gluon GPDs from such effects.

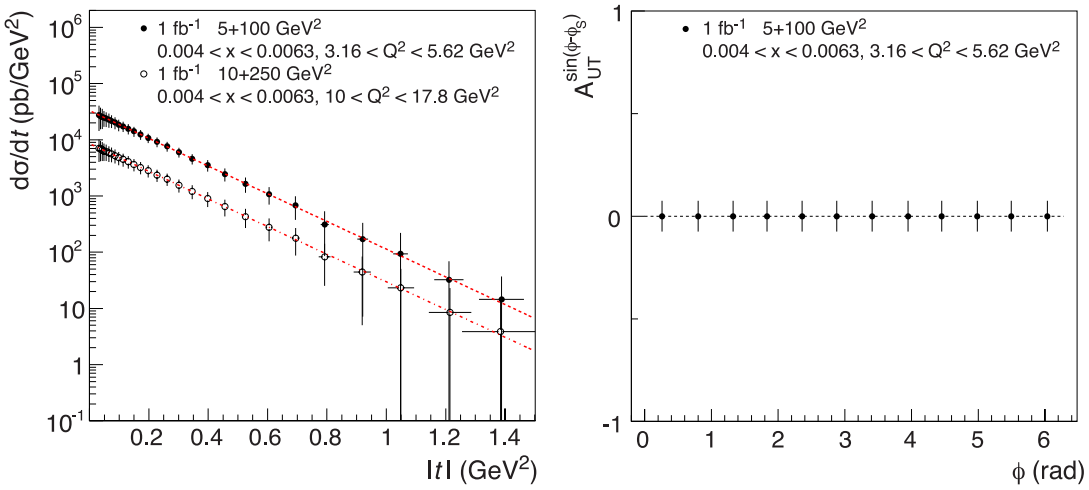

Figure 2.7: (Left) eSTAR performance for exclusive photon production in specific (x,Q^2) intervals, as indicated, for e +p collisions of 5 GeV *electron beams off 100* GeV *proton beams and of 10* GeV *electron beams off 250* GeV *proton beams. The uncertainties are the combination of statistical and systematical errors explained in text. Data sample corresponds to an integrated luminosity of* 1 fb^{-1}. *(Right) The DVCS spin asymmetry versus azimuthal angle for unpolarized electrons scattering off transversely polarized protons for the indicated (x,Q^2) interval.*

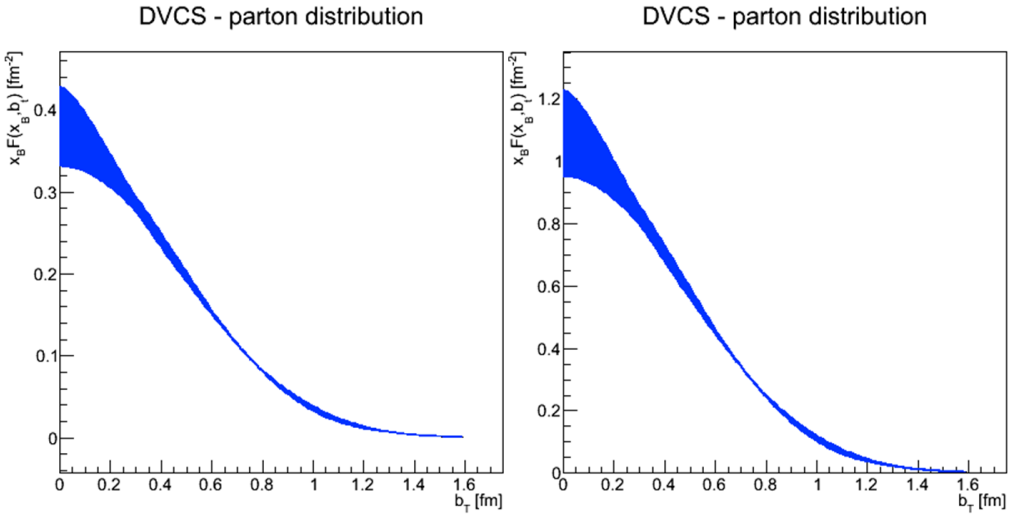

Figure 2.8: Distributions of partons in impact parameter b_T obtained from the measured DVCS cross-section results shown in Figure 2.7. Left: $0.004<x<0.0063$, $3.16<Q^2<5.62$ GeV^2; right: $0.004<x<0.0063$, $10.0<Q^2<17.8$ GeV^2. The bands represent the parametric errors in the fit of measured differential DVCS cross-section results.

The left panel in Figure 2.7 shows projections for the measurement of the differential DVCS cross-sections and transverse target spin asymmetry for 1 fb^{-1} of data collected within the eSTAR acceptance. The main background contribution to the DVCS cross-section measurements is from

the Bethe-Heitler process. The latter has been subtracted in these projections and a 3% systematic uncertainty on its contribution is propagated into the projected DVCS cross-section measurement uncertainties. Other background contributions include low multiplicity diffractive meson production and π^0/η semi-inclusive DIS production. Such background contributions were found to be negligible for the HERA experiments. They have been omitted from consideration here, since the eSTAR calorimeter has better spatial resolution in general than the calorimeters employed by the HERA experiments. Also included in the projected cross-section results is an additional 5% systematic uncertainty according to the experience of the HERA experiments. The right panel in Figure 2.7 illustrates the projected uncertainties for the corresponding DVCS spin asymmetry measurements. eSTAR is expected to have good capability also for measurements of exclusive J/ψ production in view of its electron and muon capability for mid-central rapidities. The corresponding distributions of partons in impact parameter b_T obtained from the measured DVCS cross-section results (Figure 2.7) are depicted in Figure 2.8.

Diffractive Vector Meson Production

Diffractive vector meson production, $e + p'/A' \rightarrow e' + p'/A' + V$ where $V=J/\psi, \phi, \rho$ is a unique process because it allows the measurement of the momentum transfer, t, at the hadronic vertex even in $e + A$ collisions where the 4-momentum of the outgoing nuclei can in general not be measured. Since only one final state particle is produced, the process is experimentally clean and can be identified unambiguously by the presence of a rapidity gap. The J/ψ vector meson has a compact dipole size and is thus not expected to be particularly sensitive to gluon saturation phenomena. Mesons such as ϕ or ρ, which have larger wave functions, are anticipated to be considerably more sensitive to the saturation effect.

To assess eSTAR capability for these measurements, we have carried out fast simulations using the SARTRE event generator[9] and eSTAR response parametrizations. Model settings with saturation effects result in a total cross-section of 15 μb in exclusive coherent and incoherent ϕ production in $e + Au \rightarrow e' + Au + \phi$. Instead of deriving $|t|$ from the 4-momentum of the scattered electron and the created vector mesons, an approximation is used, $|t|=(p_x^{e'}+p_x^{V})^2+(p_y^{e'}+p_y^{V})^2$, using only the transverse momenta of the particles. This approximation is found to result in good resolution with negligible bias from the true $|t|$. In addition to the kinematics, particle identification is crucial in vector meson reconstruction. STAR has unique acceptance and kaon identification for diffractive ϕ meson since the kaon momentum range is concentrated around mid-rapidity with p_T<~1 GeV as shown in Figure 3.4. Figure 2.9 demonstrates that eSTAR measurements are able to resolve the diffractive pattern. The achieved eSTAR $|t|$-resolution is projected to be approximately 2.5% (relative).

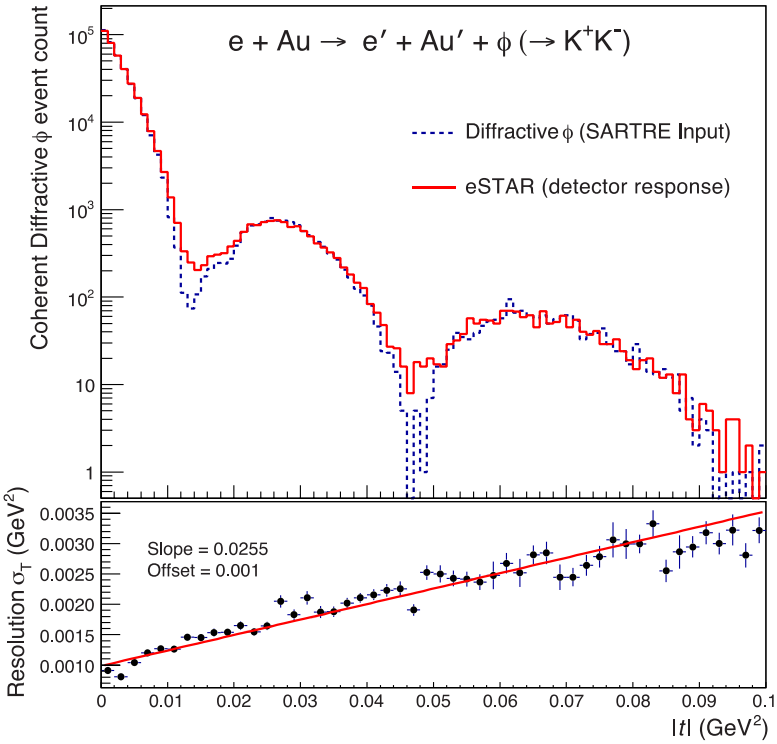

Figure 2.9: The $|t|$-spectrum for the coherent diffractive production of φ mesons in e +Au scattering in collisions with 10 GeV *electron beam energy and 100* GeV*/nucleon energy for the Au beam. The dashed line is the SARTRE generated input distribution and the solid red histogram is the result after eSTAR detector response. Ten million exclusive diffractive events were simulated. The bottom panel shows the $|t|$ resolution versus $|t|$ and is described by $\sigma_t=2.5\%|t|+0.1\%$.*

3 Detector Configuration and Components

3.1 Current Detector Configuration

Since the beginning in 2000, STAR has had a strong upgrade program to take advantage of luminosity upgrades of the machine and to enhance the physics program. The currently approved and ongoing upgrades are the Forward Gem Tracker (FGT), completed for Run13, and the Heavy Flavor Tracker (HFT), a major MIE that is projected to be ready for the STAR heavy flavor program with topological identification for Run 14. The Muon Telescope Detector (MTD) has completed over 60% of installation and is projected to be complete for Run 14, enabling a significant di-muon program alongside the heavy flavor program of the HFT. A number of additional proposals have been reviewed internally within STAR. One is to study diffractive processes in polarized $p + p$ collisions through an upgrade of the Roman Pots.

STAR mid-rapidity acceptance and particle identification capabilities, paired with more forward instrumentation aimed at high (total) energies, form key strengths into the EIC era. The STAR mid-rapidity region with the upgraded TPC, MTD, existing BEMC, and TOF is relatively well matched to the demands of inclusive and semi-inclusive deep-inelastic scattering measurements at hard scales Q^2>10 GeV^2 for the initially low electron beam-energies foreseen at an EIC. Figure 3.1 describes the current STAR detector coverage in (x, Q^2) phase space for $e + p$ ($e + A$) collisions with 10 GeV electron beam energy and 100 GeV/nucleon hadron beam energy.

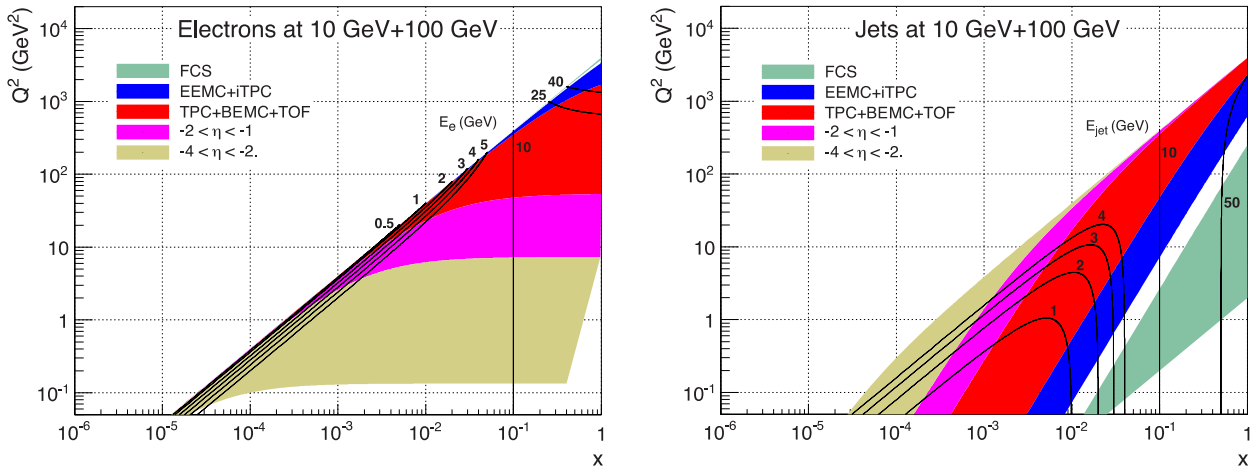

Figure 3.1: DIS kinematics of scattered electrons and jets with STAR existing detector coverage.

The extension of this coverage to smaller x or Q^2 requires forward instrumentation, in particular to identify and measure the forward scattered electron with good efficiency, purity, and resolution. Coverage over the region $-4 < \eta < -1$ (on the east end of STAR, opposite to the EEMC) would expand the Q^2 range of inclusive and semi-inclusive measurements accessible to STAR to cover essentially the entire conventional deep-inelastic regime, $Q^2 > 1$ GeV^2. The low-x region, below $x = E_e/E_h$ with $E_{e(h)}$ the electron (hadron) beam energy, is of particular interest. In this region, the

scattered electron energies range up to the electron beam energy. This holds also for the energies of the hadrons produced at backward angles in scattering of low-*x* partons. The identification of hadrons with these energies is of particular importance to semi-inclusive measurements.

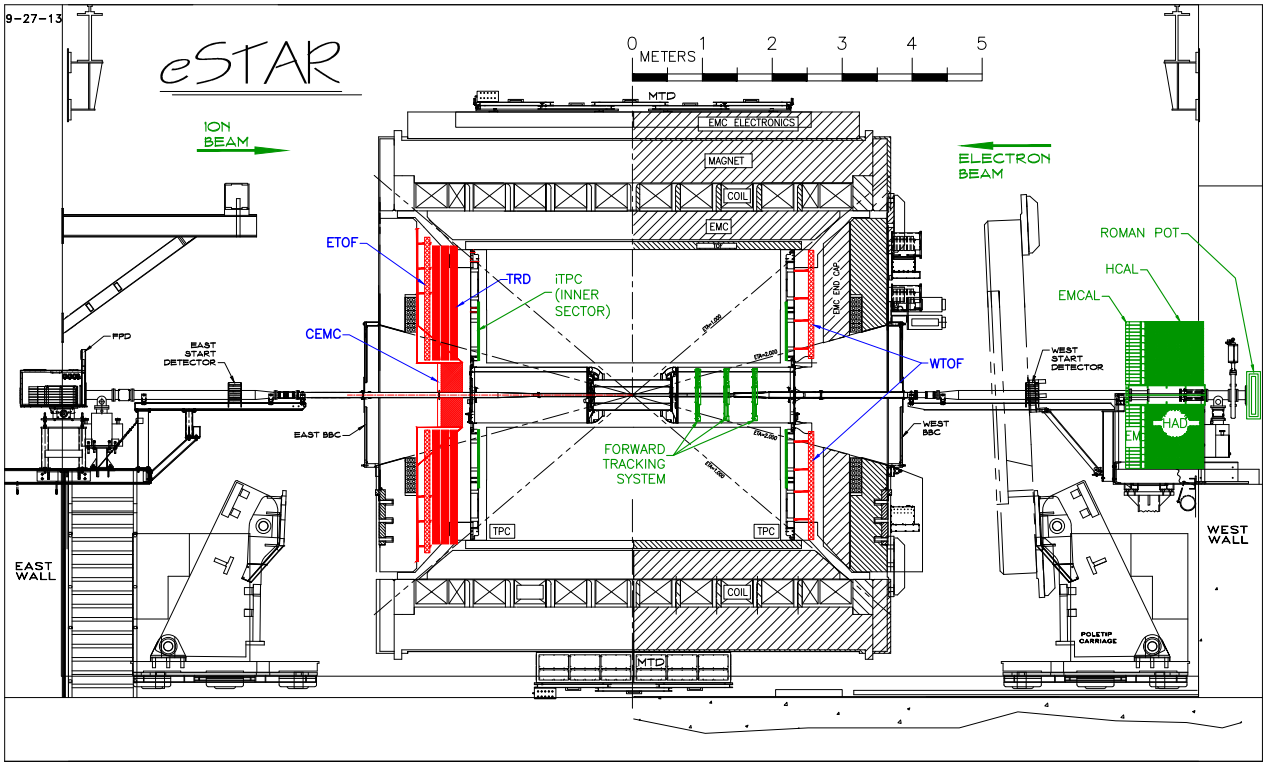

Figure 3.2: eSTAR layout with the proposed upgrades of iTPC, Forward Calorimetry System (FCS), the Forward Tracking System (FTS), Endcap TOF (E/W TOF), BSO Crystal Calorimeter (CEMC), GEM based TRD. In this configuration, the electron beam is from right to left (eastward) while hadron beam from left to right (westward).

3.2 Proposed eSTAR Detector Configuration

STAR has proposed a baseline eSTAR detector configuration for eRHIC with electron beam energy of 10 GeV and below, depicted in Figure 3.2. In addition to the major upgrades of inner TPC sectors (iTPC) and forward calorimeter and associated tracking system (FCS) before the completion of the RHIC program with STAR Detector, we have proposed a series of upgrades specifically designed for eSTAR: endcap TOF on both east and west pole-tips covering pseudorapidity of $1 < |\eta| < 2$, GEM based TRD (GTRD) ($-2 < \eta < -1$), BSO based crystal calorimeter (CEMC) and its pre-shower ($-4 < \eta < -2$).

3.3 Expected DIS Coverage and Performance

3.3.1 Resolution and Coverage of Detecting Electrons and Hadrons

Due to the asymmetry of the collisions and DIS kinematics, different components of the detector

Table 3.1: eSTAR Detector Coverage and Resolution in the pseudorapidity range.

Coverage	Orientation	Tracking	EMC	HCAL	Resolution (momentum or energy)
$-4<\eta<-2$	Electron Beam direction; EAST		BSO		$\sigma_E/E=2\%/\sqrt{E}\oplus 0.75\%$
$-2<\eta<-1$		iTPC+GTRD +ETOF			$\sigma_p/p=1/(p_T/p_Z-1/6)\times(0.45\%p_T\oplus 0.3\%)\oplus(p_Z/p_T)\times 0.2\%/p/\beta$
$-1<\eta<1$	Middle Rapidity	TPC+TOF	SMD+EMC		$\sigma_E/E=14\%/\sqrt{E}\oplus 2\%$ $\sigma_p/p=0.45\%p_T\oplus 0.3\%\oplus 0.2\%/p/\beta$
$1<\eta<1.7$	Hadron Beam direction; WEST	iTPC+TOF			$\sigma_p/p=1/(p_T/p_Z-1/4)\times(0.45\%p_T\oplus 0.3\%)\oplus(p_Z/p_T)\times 0.2\%/p/\beta$
$1<\eta<2$		iTPC+FTS	SMD+EMC		$\sigma_E/E=16\%/\sqrt{E}\oplus 2\%$
$2.5<\eta<5$		FTS	W-fiber EMC	HCAL	$\sigma_E/E=12\%/\sqrt{E}\oplus 1.4\%$ $\sigma_E/E=38\%/\sqrt{E}\oplus 3\%$

serve specific purposes in different pseudorapidities. Table 3.1 lists the detector subsystems in different pseudorapidity and their energy (momentum) resolutions. The resolutions of existing detector subsystem are obtained from the actual performance while the resolutions of proposed detectors are based on simulation and prototype test results. A series of publications outline the performance of existing detectors[4,10].

3.3.2 Particle Identification

Besides coverage and resolution, another detector quality important to the EIC program is particle identification. With the combination of dE/dx from the TPC, velocity measured by TOF and energy deposit in the electromagnetic calorimeter covering 2π azimuthal angle, STAR is an ideal collider detector for particle identification of electron, π^0 and charged hadrons. With the precise track trajectory provided by the helix in the TPC in a solenoidal magnetic field, V^0 reconstruction (the reconstruction of a displaced pair of oppositely charged particle tracks from the decay of Λ^0 hyperons and from other states) is proven to be efficient over a wide momentum range.

The measured spectra of particles in STAR include γ, e, μ, π^0, $\pi^{\pm}$, η, ρ, ϕ, $K^{\pm}$, Ks, K*, p, Δ, Λ, Ξ, Ω, $D^{0,*}$, J/Ψ and ϒ. Ref.[11] provides a complete list of STAR publications. The identified charged and neutral pion spectra have been measured in the transverse momentum range of $0.2 < p_T < 15$ GeV at $|y|<1$ for $\pi^{\pm}$ [12] and various rapidity ranges for π^0 [13]. Electron identification and hadron rejection are essential to the eSTAR physics program. At mid-rapidity $|y| < 1$, STAR has proven to be an

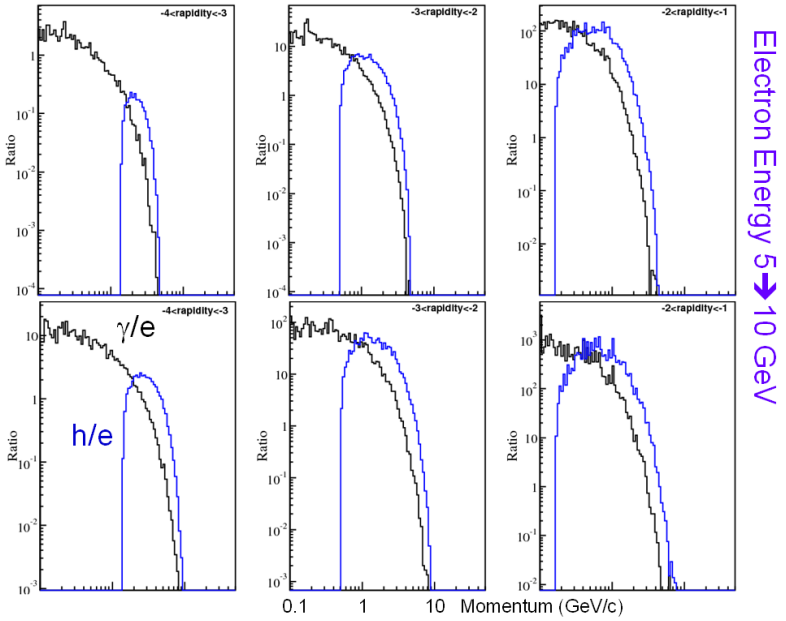

Figure 3.3: photon and hadron background to electron ratio as a function of momentum for different rapidity range in e+p collisions with electron beam energy of 5 GeV (top panels) and 10 GeV (bottom panels).

excellent detector for electron measurements with low material (<1% X_0) and large hadron rejection over a large momentum range[10]. Taking an example from the STAR publication in Ref.[14], STAR has shown to be able to achieve hadron rejection at a level better than 10^5 at $p_T = 2$ GeV. The proposed upgrade of iTPC further improves the hadron rejection by more than an order of magnitude at mid-rapidity. In addition, GTRD and ETOF upgrades are proposed to achieve the necessary electron identification in the pseudorapidity range ($-2 < \eta < -1$) in the DIS kinematics of the scattered electrons essential to the eSTAR physics program. Going even more forward in the electron scattered direction, the requirements for hadron rejection become less stringent. However, the requirement of precise measurement of electron kinematics and the need to reject photon conversion and misidentification as an electron become increasingly demanding. Figure 3.3 shows

the ratio of background photon and hadron yield to the scattered electron yield. Although the h/e ratio is about 1000 at mid-rapidity, hadron contamination is negligible and concentrated in a limited momentum range at very forward rapidity. However, the photon becomes the major source of background. We have proposed to leave only the beam pipe and its necessary support structure along this direction, and to install a crystal calorimeter and preshower to precisely determine the electron energy and angle with minimum material along the electron path. In this rapidity range, the crystal calorimeter material along the beam direction amounts to about 25 radiation length and less than one interaction length. Adequate hadron rejection factor is likely to be achievable by a combination of preshower hit position, energy deposition and shower lateral distribution in CEMC and shower leakage detected by existing Beam-Beam Counter (BBC) behind the CEMC. It is useful to note that the simulated performance of CMS Endcap crystal calorimeter[15] showed that a hadron rejection factor of 44 for low-energy electrons can be obtained by shower shape and preshower, and additional factor of 1.4 from hadron calorimeter and a factor of 5 more from track matching. Although the performance and physics properties of the CMS crystal calorimeter ($PbWO_4$) is similar to the eSTAR CEMC (BSO), the material budget of CMS tracker (up to 40% X_0) and

Table 3.2 eSTAR particle identification capabilities in different pseudorapidity.

	$e^{\pm}$	γ/π^0	$\pi^{\pm}$	$K^{\pm}$	p
$-4 < \eta < -2$	Y	Y	N	N	N
$-2 < \eta < -1$	Y	N	$0.1 < p < 15$ GeV	$0.1 < p < 3$ GeV	$0.1 < p < 5$ GeV
$-1 < \eta < 1$	Y	Y			
$1 < \eta < 1.7$	Y	Y			
$1.7 < \eta < 2$	Y	Y	N	N	N
$2 < \eta < 2.5$	Tracking without PID (charged hadrons)				
$2.5 < \eta < 5$	Y	Y	Tracking and Energy without PID		

preshower significantly impacts its performance. Instead of a hadron calorimeter behind the EMC in CMS, veto power from hits in eSTAR BBC behind the CEMC may be as effective for this purpose. This illustrates the magnitude of possible hadron rejection of eSTAR in this pseudorapidity range, and simulations of eSTAR CEMC hadron rejection power with detailed material budget is in progress.

In addition, the acceptance and identification of hadrons at low momentum is important for the diffractive vector meson sensitive to the gluon saturation effect. Figure 3.4 shows the daughter kaon momentum distribution in the exclusive process $e + \text{Au} \rightarrow e' + \text{Au}' + \phi \rightarrow e' + \text{Au}' + K^+ + K^-$,

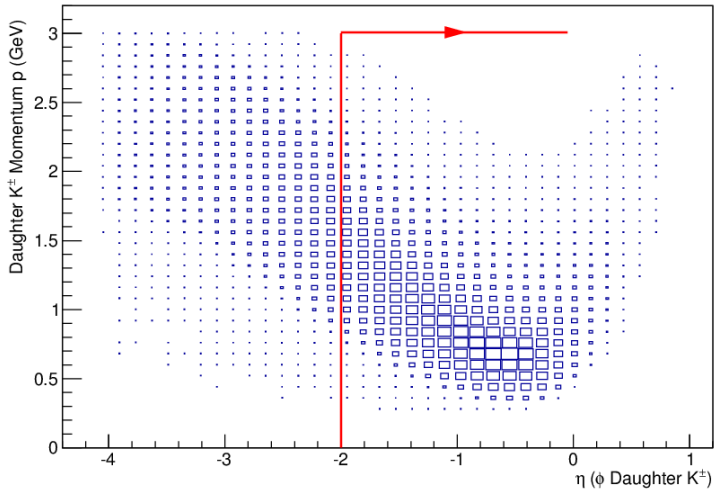

Figure 3.4: charge kaon momentum distribution as a function of pseudorapidity from diffractive ϕ production generated by SARTRE in e+Au collisions at 5×100 GeV. The red line and arrow indicate eSTAR acceptance.

illustrating the importance and strength of STAR's capability for kaon identification and acceptance at low momenta around mid-rapidity.

3.3.3 TPC Occupancy and Pile-up with eRHIC Luminosity

At the heart of the STAR detector is the Time Projection Chamber. Therefore, it is necessary to verify that STAR TPC can handle the luminosity expected in eRHIC. Table 3.3 lists the collision species of $e + p$, Au + Au, $p + p$ at 200 GeV and $p + p$ collisions at 500 GeV with luminosities achieved or projected. The TPC occupancy is characterized by the track density per unit of pseudorapidity per time interval. The results from PYTHIA $e + p$ simulation and achieved luminosity at RHIC so far show that the track density in eRHIC is over an order of magnitude lower than that achieved at RHIC. We have concluded that the STAR TPC is suitable for the EIC environment in terms of event pile-up and occupancy.

Table 3.3: STAR TPC occupancy in different collision environment.

Beam species	Beam Energies	Peak Luminosity ($cm^{-2}s^{-1}$)	Cross section (cm^2)	Nch/dη	**Track density (dNch/dη MHz)**
$e + p$	5x250	10^{34}	10^{-28}	0.7	**0.7**
Au + Au	100x100	$5x10^{27}$	$7x10^{-24}$	161	**6**
$p + p$	100x100	$5x10^{31}$	$3x10^{-26}$	2	**3**
$p + p$	250x250	$1.5x10^{32}$	$4x10^{-26}$	3	**18**

4 Detector Performance Simulations

This section will discuss the results from simulations used to predict the resolution, efficiency and kinematic coverage provided by the detectors discussed in Section 3. All of the studies presented here, with the exception of the TRD, are based on STARSIM, a simulation framework developed by the STAR collaboration. GEANT3 is used to implement the detector systems and describe interactions between particles and experimental materials. The STARSIM package has been used and tested against the STAR data for over a decade and provides a sound foundation for the eSTAR upgrade simulations. The transition radiation process is not included in GEANT3 so the TRD simulations were produced with a stand-alone package that utilized GEANT4. The deep-inelastic *e* + *p* scattering events were generated with the PYTHIA6 Monte Carlo package.

4.1 Detector Kinematic Acceptance and Efficiency

As discussed in Section 5, the inner sectors of the existing TPC will be re-instrumented with 48 readout pad rows. Figure 4.1 demonstrates the significantly improved particle reconstruction efficiency with the iTPC (red) compared to the existing TPC (blue). The coverage in pseudo-rapidity increases from $|\eta| < 1$ to $|\eta| < 1.4$, with the efficiency dropping to ~10% at $\eta = 1.6$ when 15

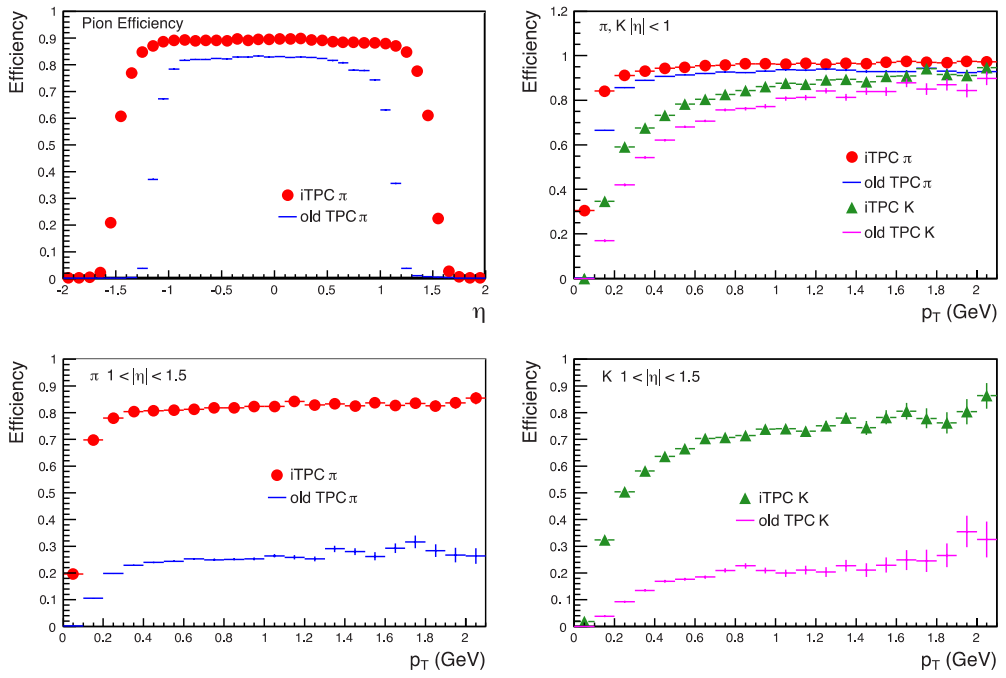

Figure 4.1: The top-left plot compares the pion reconstruction efficiency as a function of pseudorapidity for the proposed iTPC (red) and the existing TPC (blue). The top right plot demonstrates the marked improvement at lower p_T for both pions and kaons at mid-rapidity. The bottom two plots show a factor of four increase in reconstruction efficiency, for all p_T values, for pions and kaons in the forward region.

TPC hits are required along a track. For tracks with large incline angle, requirement of a track length in the TPC active volume (30 cm), equivalent to the tracks with 15 TPC hits in the middle rapidity, extends the reconstruction to η =1.7. The increased efficiency is fairly constant across particle p_T[1] and ranges from a 10-20% effect at mid-rapidity to a 300-400% increase in the forward regions. This improvement in efficiency will extend the particle reconstruction capability to lower p_T as well.

An Endcap TOF+TRD system for Identifying Electrons (ETTIE) will be installed on the electron beam side of the TPC. The TRD will perform the essential function of identifying the scattered electrons in $e + p$ and $e + A$ collisions, in addition to providing energy loss measurements and additional track points for momentum reconstruction. The ETTIE electron identification power was studied by using the hit position and total energy deposition in the Xe gas absorber of the TRD to construct a likelihood function, allowing the separation of electrons and hadrons.

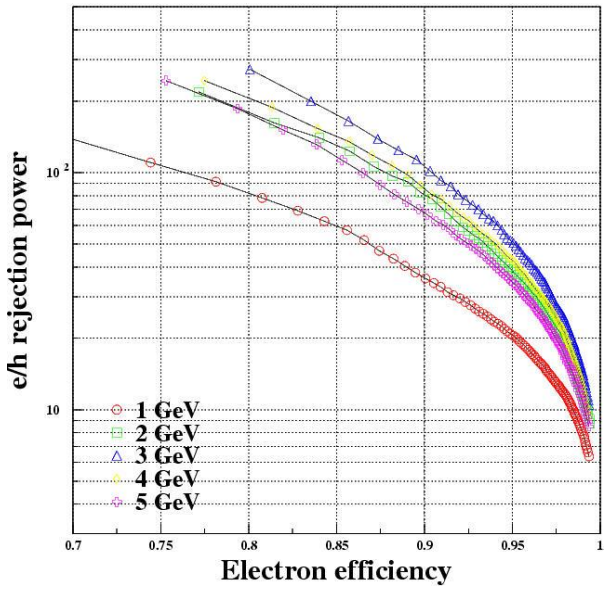

Figure 4.2: The ETTIE e/h rejection power.

Figure 4.2 shows the electron to hadron rejection power as a function of electron efficiency for different energies. At 90% electron efficiency, the rejection power ranges from about 30 to 100 depending on the energy of the electrons. The Endcap TOF information and the energy deposited in the convertor sandwiches, not included in the above studies, can be used to further increase the electron identification capability. Overall we estimate that an *e/h* rejection factor larger than 1000 can be achieved for electrons with energies from 2 to 5 GeV.

[1] The momenta p_T in this section are transverse with respect to the electron and hadron beams, not with respect to the virtual photon as is typically used in semi-inclusive deep-inelastic scattering.

The CEMC, a homogeneous electromagnetic calorimeter constructed from BSO crystals, will fill most of the acceptance between ETTIE and the beam pipe. The efficiency of the CEMC is expected to be 90%. Additional details are discussed in section 5.2.2.

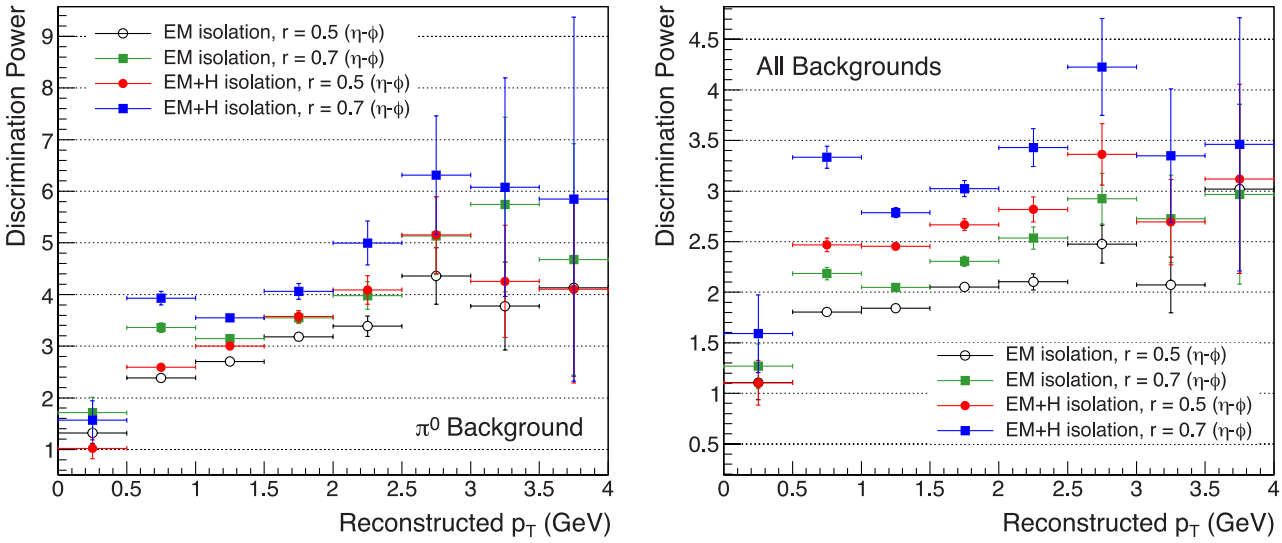

Figure 4.3: Prompt photon discriminating power in the FCS using electromagnetic only and using both electromagnetic and hadronic calorimeter isolation conditions.

The forward calorimeter system (FCS) will span the region $2.5 < \eta < 5$, with respect to the proton beam, and will allow for photon, charged and neutral hadron, and full jet reconstruction. Figure 4.3 illustrates the FCS prompt photon discriminating power. The ability to isolate prompt photons is significantly increased (~50%) for all p_T ranges when an isolation cut from the hadronic calorimeter is included.

4.2 Detector Momentum and Energy Resolution

The p_T resolution with the iTPC upgrade is shown in Figure 4.4. The purple curve in the left panel shows the resolution for the current TPC detector in a realistic luminosity and pile-up environment at mid-rapidity. The open squares and fit indicate a marked improvement from 0.45% to ~0.2% resolution due to reconstruction with the iTPC upgrade and additional beamline constraints. At higher $p_T > 1$ GeV, the resolution increases linearly with momentum, but degrades at low p_T due to multiple Coulomb scattering. The right plot demonstrates how the linear resolution term varies with η, ranging from 0.4% at $\eta = 1$ to 1.7% at $\eta = 1.6$.

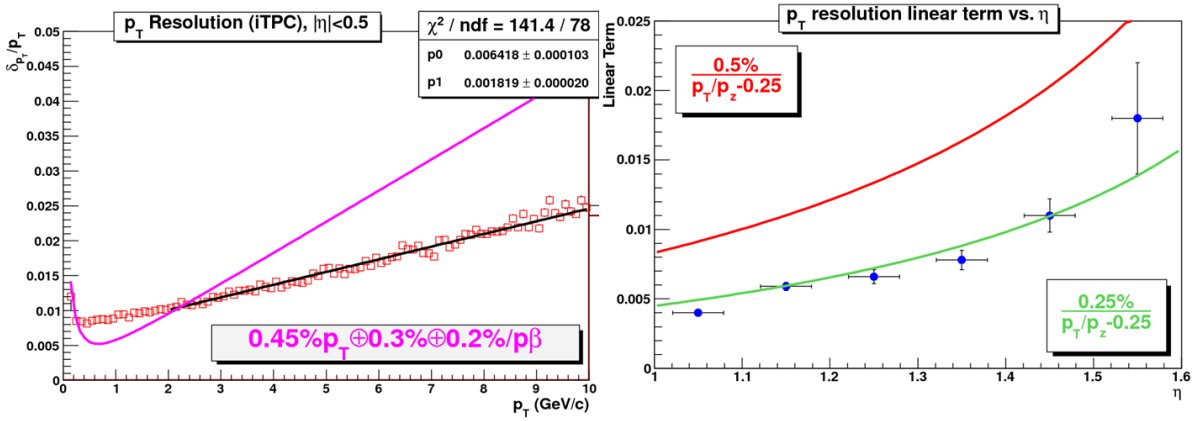

Figure 4.4: (Left) reconstructed particle p_T resolution in the TPC (purple curve) and iTPC (open squares) at mid-rapidity and (right) as a function of η.

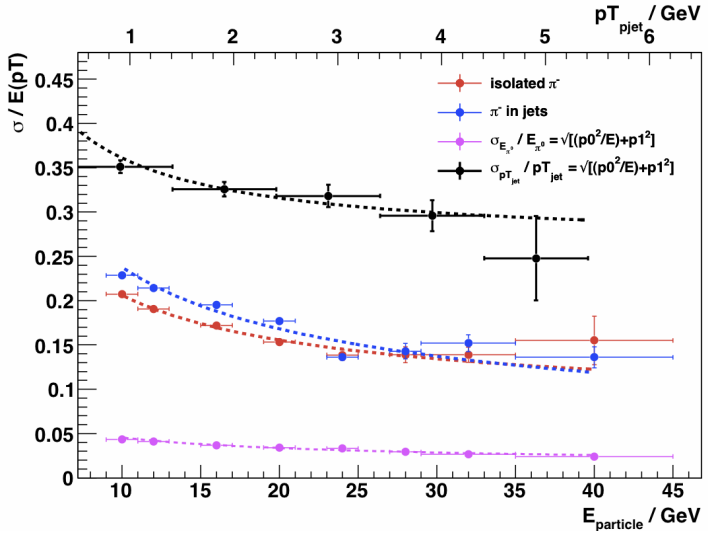

Figure 4.5: Resolutions for charged (red and blue) and neutral (pink) pions as a function of the generated energy (bottom axis). The jet resolution is plotted versus jet p_T (top axis).

Figure 4.5 shows the simulated charged and neutral pion energy resolutions in the FCS as a function of the initial energy of the thrown particle. The energy resolution is largely determined by the hadronic calorimeter and ranges from 24%/$\sqrt{E}$ at E = 10 GeV to 14%/$\sqrt{E}$ at 40 GeV for the charged pions. The jet p_T resolution is of similar scale and ranges from 24% to 18% for p_T = 1-6 GeV.
The CEMC energy resolution for photons and electrons is estimated to be similar with that of PANDA EMC based on PWO (cooled) crystals, which is anticipated to be 2%/$\sqrt{E}$ ⊕ 0.75%.

4.3 DIS Kinematics Reconstruction at eSTAR

Figure 4.6 illustrates the x, y and Q^2 resolution in deep-inelastic scattering collisions of a 10 GeV electron beam off a 100 GeV proton beam as reconstructed with the eSTAR iTPC, ETTIE, and CEMC. The detection efficiency for the scattered electron is largest in the region of $5\text{x}10^{-4} < x <$

$5x10^{-2}$. The narrow inefficiency indent at Q^2~=0.8 GeV^2 and x between 0.01 and 0.1 is due to the lower efficiency when both iTPC (~90%) and GTRD (~90%) hits are required. The x resolution is proportional to $1/y$ when only the scattered electron observables are used in the reconstruction of the event kinematics and, at constant Q^2, thus becomes worse with increasing x. The Q^2 resolution is

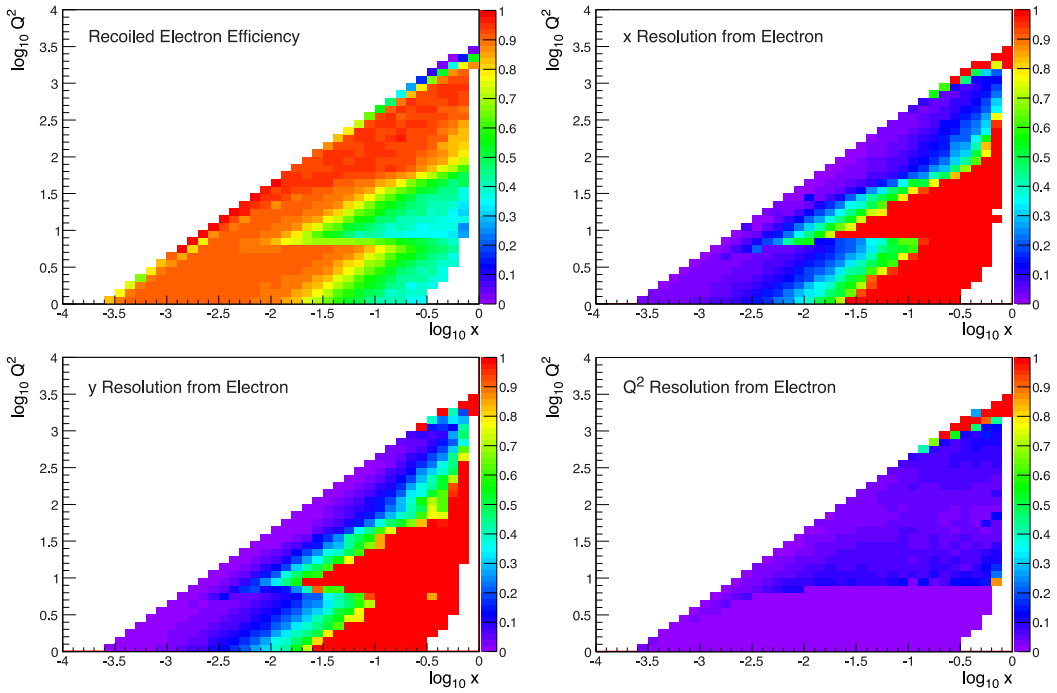

Figure 4.6: (Upper right) electron detection efficiency and percentage resolution in (upper right) x, (lower left) y, and (lower right) Q^2 for deep-inelastic scattering of a 10 GeV *electron beams off a 100* GeV *proton beam.*

better than 20% and is fairly uniform across the entire electron reconstruction region.

5 Proposed Upgrades and R&D

Research and Development projects are the first steps toward realizing a cutting-edge detector. STAR's past R&D projects have resulted in new measurement capability at central and forward rapidity. Every detector component proposed in this LoI has an associated and active R&D effort. Several of the projects have benefited, or are benefiting, from the generic detector R&D program organized by BNL in association with JLab and DOE to address the scientific requirements for measurements at a future EIC. This section will give a brief description of the ongoing R&D projects that were motivated and studied in simulations in the previous sections.

5.1 Major Upgrades to STAR before eRHIC

5.1.1 Inner TPC Sector Upgrade (iTPC)

STAR plans to upgrade the inner sectors of the TPC (iTPC) to increase the instrumentation of the inner pad plane and to renew the inner sector wires, which have accumulated significant radiation dose in more than a decade of RHIC operation and are considered to have potential aging effect. The new inner sector pad-planes will replace the old planes, which have only 20% coverage of the fiducial volume. A reconfiguration of the RDOs and FEEs is being considered, such that they will be inserted along the sector boundary, to reduce the material in the fiducial area. The upgrade will provide better momentum resolutioies, better dE/dx resolution, and most importantly it will provide improved acceptance at high rapidity to $|\eta| < \sim 1.7$ compared to the current TPC configuration that covers $|\eta| < \sim 1.0$. Increased acceptance at higher rapidity is a crucial part of STAR's future physics programs, including in particular the second phase of the Beam Energy Scan program (BES II).

The iTPC hardware upgrade will impact four components, namely, the inner pad planes, the multi-wire proportional chambers, the read-out (RDO) and front-end electronics (FEE), and the sector support strong-backs. The iTPC upgrade aims to:

- provide hermetic read-out coverage in the fiducial gas volume,
- eliminate the effects of potential wire-aging incurred during RHIC operations,
- reduce ion leakage between the inner and outer sector boundaries,
- reduce the material in the support structure and strong-backs in the inner sectors.

Ongoing R&D[16] is aimed at finalizing the mechanical structures and the layout of the pad plane for incorporation in the upgrade proposal.

5.1.2 Forward Calorimeter System (FCS)

The envisioned forward instrumentation upgrade will enable STAR to measure photons, neutral pions, electrons, hadrons and jets in the forward rapidity region between $2.5 < \eta < 5$. The kinematics of two-to-two parton scattering in hadron-hadron collisions result in sensitivity to high and low values of Bjorken-x at forward rapidity. Initial Monte Carlo simulations, discussed in

section 4, indicate that the proposed FCS will provide good photon and neutral pion separation, electron identification and hadron rejection, and jet energy resolutions.

The Forward Calorimeter System (FCS) consists of a Spaghetti electromagnetic Calorimeter (SPACal), followed by a Lead and scintillator plate sampling Hadronic Calorimeter (HCal). The SPACal will be made of Tungsten powder and Scintillating fibers in spaghetti geometry. The novel SPACal detector construction technique has been developed by a team from UCLA/TAMU/PSU through an EIC generic detector R&D project. The proposed SPACal has 120x80 towers each approximately 2.6x2.6x17 cm^3 corresponding to 24 X_0 lengths. Figure 5.1 shows the resolution determined from data taken with a prototype module that was exposed to a test-beam at FNAL early in 2012 in comparison with the resolution obtained from simulations.

The HCal section will be made of lead and scintillating tiles with each 10x10x81 cm^3 tower corresponding to 4 interaction lengths. The HCAL will be composed of a 30x20 tower array, covering the same area as the SPACal. A novel construction technique will be investigated to build the detector by stacking the tiles in-situ to allow for smooth mechanical integration in STAR. STAR is considering also the option of re-using the E864 calorimeter after validation of its performance as a part of the HCal system.
The readout of the SPACal will be located on the front of the module, while the readout of the HCal

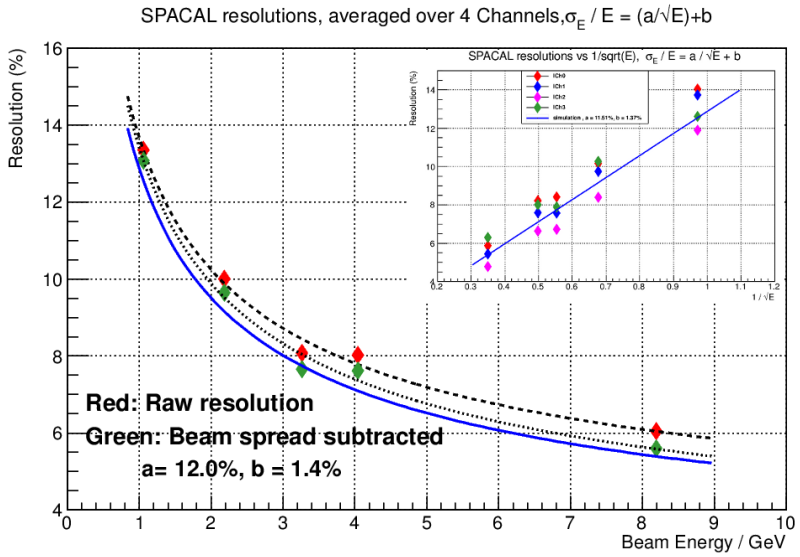

Figure 5.1: Test beam results of prototype Tungsten fiber calorimeter at FermiLab. Shown are energy resolutions as a function of incident electron beam energy (dashed lines fitted to data) in comparison to GEANT simulation (blue line).

will be situated at the rear end of the module. There will be no space gap between the SPACal and the HCal. The ratios of the tungsten/scintillator for the SPACal and the lead/scintillator for the HCal are designed to ensure approximately the same responses from electrons and hadrons. The SPACal has a very fine segmentation and the dimensions of the tower are chosen to match the Moliere

radius of the tungsten/scintillating-fiber SPACal. Silicon PhotoMultipliers (SiPM) will be used as photon sensors for both the SPACal and the HCal detectors.

STAR has initiated an R&D project[17] to construct a full-scale prototype of the FCS module. Major goals of the R&D include the establishment of the HCal detector construction technology, optimization of the photon readout scheme, and measurements of the detector performance in a test beam run. Simulations are in progress and a beam test-run at FNAL is scheduled in 2014.

5.2 eSTAR Specific Upgrades and R&D

In addition to the iTPC, FCS and FTS upgrades prior to eRHIC, STAR is pursuing two major R&D projects aimed at extending STAR's capabilities into the eRHIC era:

- An Endcap TOF and TRD for Identifying Electrons at EIC (ETTIE), and
- Crystal Electromagnetic Calorimeter for forward electron identification and measurement at EIC (CEMC).

5.2.1 Endcap TOF and TRD for identifying electrons (ETTIE)

The ETTIE detector aims to provide electron identification with high hadron rejection (~>10^3) over a wide momentum range (0.2 GeV < p < ~10 GeV) by combining a MRPC-based Time-of-Flight detector (TOF) and a GEM-based Transition Radiation Detector (TRD) in the forward electron direction (-2 < η < -1). ETTIE will be located between the low material TPC tracking detector and the pole-tip, and will provide additional tracking points comparable to the TPC hit precision for hadron reconstruction as well as the start time for hadron detection in other areas of the TOF acceptance. Simulations indicate that the combination of ETTIE + iTPC is likely to provide a cost-effective detector system for extending STAR's excellent electron identification and tracking out to η = -2. In the case of a 5 GeV electron beam, the setup will provide complete coverage for Q^2 > 1 GeV^2 in e + p and e + A collisions for a first-stage eRHIC detector.

A generic EIC R&D project[18] is being carried out to use GEM detectors in combination with a Xe+CO_2 volume for the detection of transition radiation. This will allow further evaluation of the feasibility of ETTIE for eSTAR. The ongoing R&D goals are to study the GEM readout performance for dE/dx (transition radiation) signals and position resolution and to investigate the impact on tracking and dE/dx of regular and thick GEM configurations. Figure 5.2 shows a schematic of a GEM-based TRD and results from a GTRD prototype in a cosmic-ray test-stand.

The Endcap TOF subsystem in ETTIE is equipped with MRPC technology, and the R&D plans to use custom electronics based on a CERN HPTDC that was successfully used in the STAR barrel TOF and MTD sub-systems. This configuration should provide very high-resolution timing information, resulting in an overall TOF time resolution of 70 to 100ps. In phase-II of the ETTIE R&D STAR will investigate the radiation and rate capabilities of the TOF prototype detectors, as

well as electronics options and the effects of installation inside a realistic magnetic and radiation environment (e.g. between the STAR TPC sectors and the pole-tip).

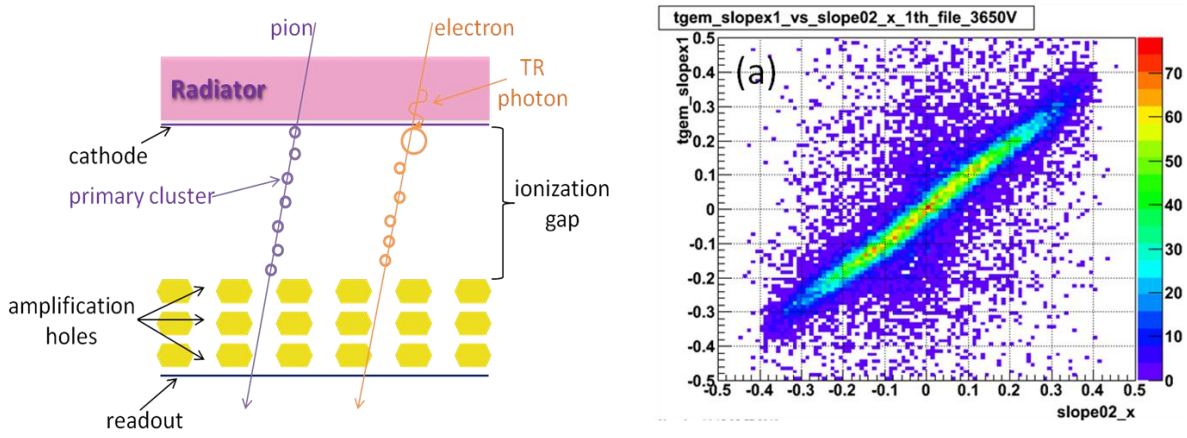

Figure 5.2: (Left) schematic of GEM based transition radiation detector and (right) tracklet slope measured with a GTRD prototype vs slope from two regular GEM detectors placed on top and bottom of the GTRD prototype in a cosmic ray test stand. The results show that the GTRD prototype has good position (300µm) and angular resolutions.

5.2.2 Crystal Calorimeter based on BSO (CEMC)

Enhanced forward acceptance is essential in collisions with 10 GeV electron beam energies, as well as for lower Q^2 physics with electron beam energies of 5 GeV. The rate of electrons scattered forward into this acceptance region is similar to the rate of hadrons is this region and at these energies. A crystal calorimeter with 2-3% energy resolution for 2-5 GeV electrons is expected to be a suitable detector technology for electron identification at these energies. Crystal detectors with

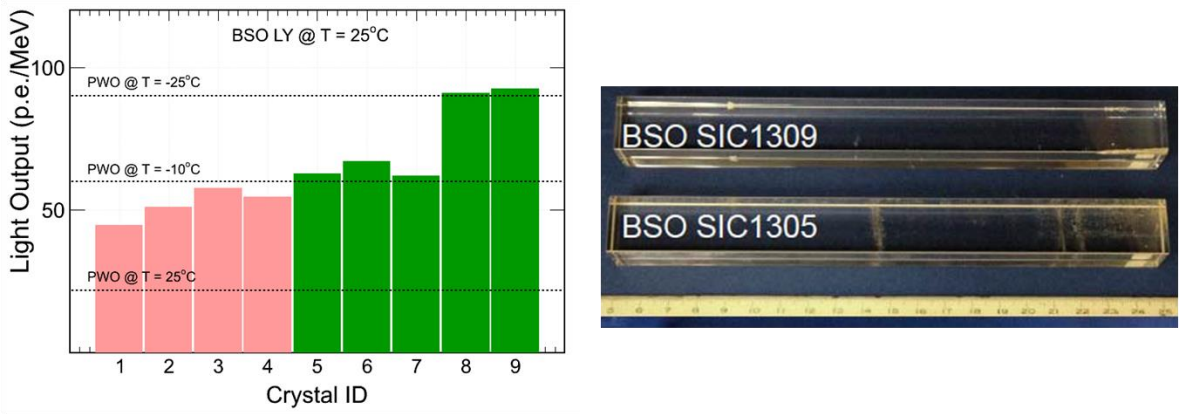

Figure 5.3: Light output of BSO crystal produced by SCCAS in Shanghai. The light yields of last two produced crystals at room temperature were measured to be similar to the PWO at temperature of -25C. Right panel shows the two crystals (ID#5,9 in left panel. The dimensions of the crystals are 2x2x20 cm^3*).*

good energy resolution have been used extensively in other experiments both to identify and trigger on electrons and photons. STAR is proposing to use a forward calorimeter with BSO crystals. BSO crystals at room temperature have comparable light yield as PWO at low temperature (-25^{o}C) with significantly lower cost. A BSO calorimeter will provide a cost-effective electromagnetic calorimeter for electron measurement in the region of $-4 < \eta < -2$. A generic EIC R&D project has been conducted by collaboration between USTC, one of the institutes in STAR, and the Shanghai Institute of Ceramics, Chinese Academy of Sciences (SICCAS). Shanghai SICCAS High Technology Corporation, a research-based enterprise wholly invested by SICCAS, is able to supply crystals with high quality for worldwide customers that are especially suitable for crystal detectors in high energy experiments, such as those at Jefferson Lab (USA), KEK (Japan), INFN (Italy), PANDA (Germany). The group has produced a set of 3x3 BSO crystals, each with dimensions of 2x2x20 cm^3. Preliminary tests show high light output, as expected. Figure 5.3 shows that the light yields have improved significantly over time with improved production procedure and crystal purity. The CEMC calorimeter will require about 1500 high-quality crystals. The CEMC triggering capabilities will be further investigated.

5.3 Other Upgrades and planned R&D Activities

STAR's ability to achieve many of the forward physics goals, both before and during the eSTAR era, will rely on the implementation of fast forward tracking system (FTS) for charged particles in the $2.5 < \eta < 5$ region. Charge-sign separation and good spatial resolution for charged-particle tracks that will enable accurate pointing towards the calorimeters, are both required. The momentum resolution will inevitably be limited by the small integrated $\int Bdl$ in the 0.5 T solenoidal magnetic field for small-angle scattering. STAR is currently comparing the benefits of both Microstrip Silicon detectors (technology used by CMS) and GEM-based trackers for these purposes. In the GEM-based variant, the existing Forward-GEM-Tracker (FGT) would be complemented with 5 to 6 additional disks of similar geometry. In the silicon variant, three disks are envisioned that will replace the FGT and enable measurements in the $A+A$ collision system. Several groups are pursuing GEM-based R&D under the auspices of generic EIC R&D. STAR intends to engage also in R&D aimed at Si-based tracking.

STAR is completing the Heavy Flavor Tracker (HFT) project, which is essential to the RHIC physics program in the coming decade. The current HFT configuration has the dominant part of its support structures and utilities on the east side of STAR in the pseudorapidity range of $-2 < \eta < -1$. In the eRHIC era, this acceptance range is vitally important to measure the scattered electron. STAR is considering several options for the eSTAR inner tracking system that would meet this requirement and also enable a heavy flavor program with displaced-vertex detection:

- a reconfiguration of the HFT so as to relocate the support structures and utilities,
- a 180^{o} rotation of the HFT structures so that they will occupy the west side of the detector, which has comparatively less stringent demands on the material budget,
- the relocation of the HFT and the addition of a compact mini-TPC on the east side.

In any of the above options, which are not part of the current eSTAR baseline concept, the HFT sensors will be replaced with a future generation of sensors to make optimal use of the continued development of, in particular, the MAPS sensor technology.

The envisioned suite of detector upgrades will require commensurate evolution of the existing STAR trigger and data-acquisition systems as has been outlined in the STAR decadal plan[1]. Techniques to measure luminosity and polarization at eRHIC and required R&D have been outlined in the EIC community whitepaper[3].

6 Collaboration Evolution

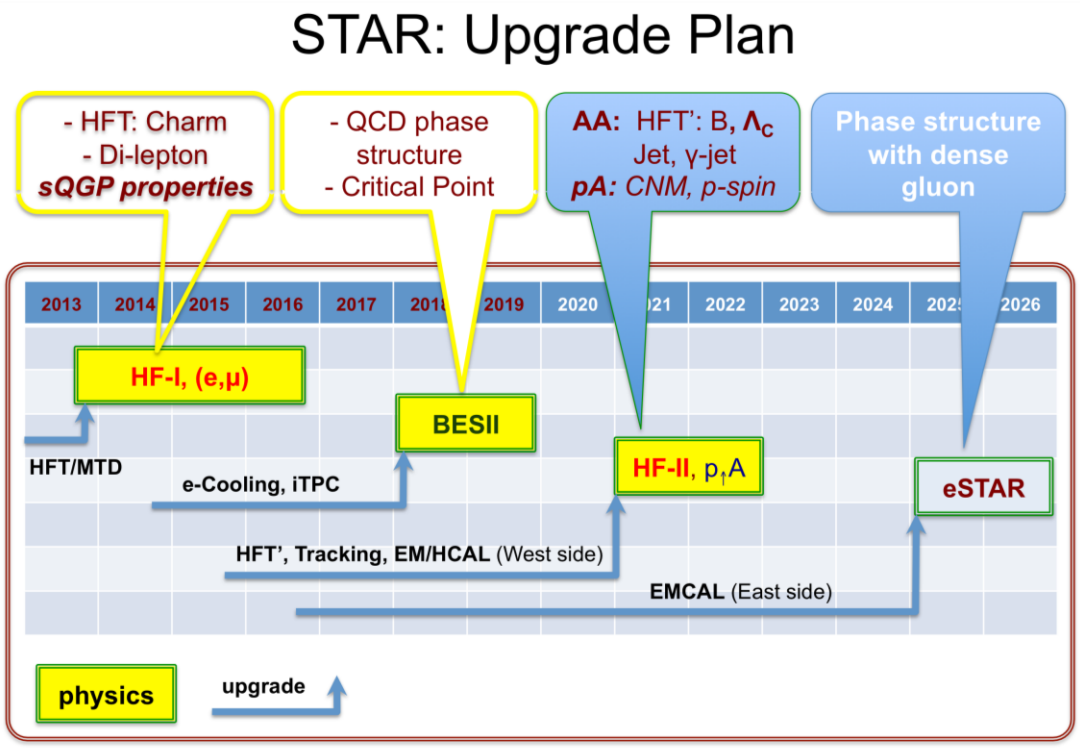

Figure 6.1: STAR's future physics programs: 2014-16, studying sQGP properties with heavy flavor and di-leptons; 2018-19, RHIC beam energy scan, narrowing in on the region of $\sqrt{s_{NN}} \leq 20$ *GeV; 2021-22, (a) sQGP properties with the upgraded faster Heavy Flavor Tracker, specifically for the measurements of bottom and* Λ_C*, and (b) polarized p + p / p + A program at the forward-rapidity region; 2025 and beyond, starting of the e + p and e + A program.*

As is illustrated in Figure 6.1, the STAR collaboration is pursuing three well-defined and focused physics programs prior to the presumed turn on of eRHIC in 2025. These programs allow the collaboration's emphasis to evolve smoothly from the study of sQGP properties, the QCD phase structure, and proton spin structure at mid-rapidity, to a physics program enabled by new forward instrumentation and ultimately the polarized *e + p* and *e + A* physics programs at eRHIC.

The initial phases of the overall physics program focus on the hot QCD properties. These studies will continue early in the next decade with the new capabilities of a faster Heavy Flavor Tracker and be complemented by studies of cold nuclear matter effects with polarized proton beams at RHIC energies and new instrumentation to access the low-*x* region of high gluon density.

We emphasize that, while we anticipate that the details of the plan will continue to evolve in the process, the integrated approach aims to optimize the unique capabilities of the RHIC facility and STAR experiment to advance QCD physics. Each phase of the program is a stepping stone for the

next and each program is executed along with upgrade projects for the next phase. At the end of the heavy-ion and polarized proton program at RHIC, with high precision, we will be able to study the QCD phase diagram over a wide range of baryonic-chemical-potential ($20 \leq \mu_B \leq 700$ MeV), the properties of the sQGP – the hot QCD matter, gain understanding of the internal spin structure of the proton and of nuclear matter at extremely large gluon density – cold nuclear matter properties. We will be able to elucidate the underlying dynamical evolution from the cold nuclear matter to the hot QGP created at RHIC.

At present, the STAR collaboration consists of 53 active institutes and 25 of them are from the United States. The majority of the collaboration is strongly supportive of the eSTAR effort and is starting to engage in the forward-upgrade and/or eSTAR efforts. Due to their commitments towards relatively new LHC projects, a large fraction of European and Indian institutes have thus far not been involved directly in STAR's future projects. In order to expand and strengthen the efforts on the forward upgrades and eSTAR, we need to engage additional institutes both from within and outside the STAR collaboration, including in particular those from the deep-inelastic-scattering community. A vibrant *p + p* and *p + A* physics program plays an integral and natural part in *maintaining, training,* and *growing* the scientific community for *e + p* and *e + A* physics programs with eSTAR at eRHIC.

Table 6.1: Project cost estimates in current year funds for the baseline eSTAR detector with the major upgrades between 2017 and 2025. Only the total project cost estimates are given for the upgrades in the eRHIC era.

Upgrade projects	Year of completion	Total project cost (M$)	Funding Sources	Supplemental information
iTPC	2017	5.5	potentially significant foreign in-kind contribution	Foreign in-kind contribution
FCS	2020	15		50% from refurbishing E864 HCAL
FTS	2020	4.5		GEM or Silicon
HFT'	2020	3		faster PIXEL chips
CEMC +preshower	2024	5		Generic EIC R&D
ETOF+WTOF	2024	4		STAR TOF/MTD
GTRD	2024	5		Generic EIC R&D
Total (M$)		42		FY 12 Dollars

The major upgrade projects necessary for the baseline eSTAR instrument are listed in Table 6.1.

The project costs and the funding profile are based on the following:

- The iTPC project has three-year duration in a technically driven schedule. Its initial physics purpose is the second stage of the RHIC Beam-Energy-Scan program, which is anticipated to start in 2017. The labor costs are projected to amount to $2.0M in this case and fabrication to $1.8M. A 45% contingency is assumed in the total. The chambers are proposed to be produced by collaborating institutions, Shandong University and the Shanghai Institute of Nuclear and Applied Physics, using strong-backs machined at the University of Texas in Austin or in China. The readout is based on the STAR DAQ1000 upgrade model and new FEE chips developed for the ALICE upgrade. The read-out costs are projected to be $1.7M, including 20% contingency and 50% overhead, and are the requested new DOE funds for the iTPC upgrade.
- The FCS project has a three-year construction period preceded by a 1-2 year design, engineering, and prototype phase in a technically driven schedule. It will initially serve measurements at forward rapidity in $p + p$, $p + A$, and $A + A$ in the later part of the decade. The labor costs are $1.9M in this case and detector material are projected to amount to $1.3M for the hadronic section and $1.4M for the electromagnetic section. The readout is costed at $1.9M. The total FCS project cost amounts to $15M including $0.6M integration costs, 40% contingency and on average 40% overhead. Significant cost saving may be possible with the option of refurbishing the E864 calorimeter after validation of its performance as a part of the HCal system.
- The FTS project is at an earlier stage of development than the iTPC and the FCS projects. Two options are being considered, using either GEM or Silicon microstrip technology. The project total cost estimate given in Table 6.1 is based on the silicon option of about 130K readout channels and is based on experience with the Intermediate Silicon Tracker (IST) subsystem of the ongoing Heavy Flavor Tracker upgrade. It contains $1.4M for detector modules, $0.3M in mechanics, $0.7M for electronics, and 30% contingency and 40% overhead. It is planned to be used for $A + A$, $p + p$ and $p + A$ physics with an envisioned timeline are similar to that of the FCS.
- The HFT' is a suggested upgrade to the existing PXL sub-system for the HFT to strengthen the proposed $A + A$ and $p + A$ programs around year of 2020. It is envisioned to be a replacement of the sensors with faster readout and less pile-up than the current readout system for the PXL without any change in the mechanics. The projected cost is based on the HFT actual costs for this component. Its implementation clearly also relies on sensor development on-going at IPHC, Strasbourg.
- The End-Cap Time-of-Flight disks, ETOF and WTOF, are an integral part of the eSTAR baseline instrument. They cover a total area that is half the size of the existing $8M STAR Barrel TOF subsystem. The projected cost is $4M, consisting of $1M for the detector, $1M in mechanics, and $2M in electronics. These include labor, 30% contingency, and on

average 40% overhead. Their construction, and the construction of the other eSTAR specific upgrades, is anticipated to start after the FCS and FTS have been completed and take 3-4 years.

- The GEM-based TRD, which together with the ETOF forms ETTIE, has a surface area that is eight times smaller than the ALICE TRD and is proposed to use electronics similar to the iTPC. The projected cost total is $5.0M, consisting of $1.0M for the detector, $0.7M in labor, and $1.7M for electronics, and assuming 40% contingency and 40% overhead.
- The CEMC + preshower costs are projected to be $5.0M in total, based on vendor costs of $1.0M for 1500 BSO crystals each with a volume of $2x2x20cm^3$, $0.3M in electronics scaled from the corresponding cost projection for the FCS, $0.4M in mechanics, $0.7M in labor, and 40% contingency and 40% overhead.

We estimate the total project costs from 2017 to 2025 to amount to $42M in current FY 12 dollars. The detector configuration presented in this Letter of Intent provides the baseline eSTAR instrument and we continue to anticipate and welcome science-driven proposals and ideas to further strengthen the eSTAR instrument, collaboration and physics capabilities.

Appendix: Charge for the eSTAR Letter of Intent

Charge to PHENIX and STAR Collaborations: LOI for Transition to eRHIC

In 2010 the PHENIX and STAR collaborations each generated decadal plans laying out proposed science goals and detector upgrade paths for the period 2011-2020. At the request of ALD Vigdor, the Decadal Plan documents provided by both collaborations included conceptual ideas for utilizing these detectors for the study of ep and eA collisions in an early stage of the eRHIC program. In the case of PHENIX, the subsequent sPHENIX proposal includes a more extensive discussion of a possible ePHENIX upgrade through inclusion of additional particle identification and forward detectors.

We now have an EIC White Paper with a comprehensive outline of the physics questions for an Electron Ion Collider, a rapidly maturing machine design for eRHIC, and a clearer view of a possible path to an early-stage eRHIC program leading to first measurements in the mid-2020s. Therefore, the PHENIX and STAR Collaboration are now being asked to consider their role in a transition from RHIC to eRHIC on this time scale, and to provide specific plans (i.e. Letters of Intent) to upgrade/reconfigure the detectors from their present form to first-generation eRHIC detectors. These Letters of Intent (LOI) will be an important part of BNL's strategic planning as we move toward the next Nuclear Physics Long Range Plan. They should include an assessment of how the collaborations may evolve through this transition, and of the size and breadth of the scientific staffing required to carry out these plans.

In preparing these LOI the collaborations should assume an eRHIC machine with an electron beam energy up to 10 GeV, hadron beam energies as provided by the current RHIC machine (255 GeV for p and 100 GeV/nucleon for Au), and design luminosities of 10^{33} cm^{-2} s^{-1} for 10 GeV on 255 GeV ep collisions and the equivalent of 6 × 10 cm^{-2} s^{-1} for 10 GeV on 100 GeV/nucleon eA collisions.

The LOI should include a description of the physics reach of the upgraded detectors, based on their detection capabilities, taking into consideration the key measurements identified in the EIC White Paper for Stage 1 (but now for 10 GeV electrons instead of 5 GeV). Further details of the desired detector requirements will be soon posted by the eRHIC Task Force on a Wiki page.

The technical details of the proposed upgrades should be given in sufficient detail to make a preliminary cost estimate. We assume that the upgrades may come in stages, with some elements implemented during the on-going RHIC heavy ion operations. Sufficient detail should be provided for each step to allow a rough outline of the overall construction schedule, assuming a 2–3 year shut-down of collider operations before the commencement of eRHIC operations, and an estimate of the required funding profile.

The Letters of Intent should be submitted by September 30, 2013. A brief statement of progress by each collaboration at the time of the June 2013 PAC meeting would be appreciated.

References

[1] STAR Decadal Plan, http://www.bnl.gov/npp/docs/STAR_Decadal_Plan_Final[1].pdf
[2] NSAC Long Range Plan (2007), http://science.energy.gov/np/nsac/
[3] A.A. Accardi *et al.*, arXiv:1212.1701 (2012).
[4] K.H. Ackermann et al. (STAR Coll.), Nucl. Instrum. Meth. **A499** (2003) 624.
[5] D. Kharzeev, E. Levin, and L. McLerran, Nucl. Phys. **A748** (2005) 627.
[6] C. Marquet, B. Xiao, and F. Yuan, Phys. Lett. **B682** (2009) 207.
[7] F. Dominguez, B. Xiao, and F. Yuan, Phys. Rev. Lett. **106** (2011) 022301.
[8] E. Perez, L. Schoeffel, and L. Favart, hep-ph/0411389v1 (2004).
[9] T. Toll and T. Ullrich, arXiv:1307.8059 (2013).
[10] M. Shao *et al.*, Nucl. Instrum. Meth. **A558** (2006) 419.
[11] STAR journal publication database, https://drupal.star.bnl.gov/STAR/publications/
[12] STAR Collaboration, Phys. Rev. Lett. **108** (2012) 72302; Nucl. Instrum. Meth. **A614** (2010) 28.
[13] STAR Collaboration, arXiv:1309.1800 (2013).
[14] STAR Collaboration, Phys. Rev. **D83** (2011) 52006.
[15] CMS note 1997/010, Low p_T electron identification in CMS, (1997)..
[16] J. Dunlop *et al.*, iTPC – An Upgrade to the TPC Inner Sector Pad Planes, (2012).
[17] J. Dunkelberger *et al.*, Prototyping for a STAR Forward Calorimeter System (FCS), (2012).
[18] Z. Xu and M. Shao, ETTIE EIC R&D proposal, (2011).